Letter of Intent:
Precise measurement of neutrino interactions and sterile neutrino search with nuclear emulsion detector at J-PARC

S. Aoki[a], D. Barčot[b], T. Fukuda[c,*], M. Ghosh[b], S. Han[d], T. Hayakawa[c], Y. Hayasaka[c], Y. Hayato[e], L. Halić[b], Y. Hirobe[c], H. Inamoto[c], G. Iwamoto[c], S. Ito[f], C. Jesús-Valls[g], A. Kasumi[c], T. Katori[h], T. Kawahara[c], T. Kawanago[c], T. Kikawa[d], B. Kliček[b], H. Kobayashi[c], R. Komatani[c], M. Komatsu[c], T. Matsuo[c], S. Mikado[i], A. Minamino[f], Y. Morimoto[c], K. Morishima[c], Y. Nakamura[c], T. Nakano[c], T. Nakaya[d], N. Naganawa[c], T. V. Ngoc[d], S. Ogawa[j], H. Oshima[e], N. Otani[d], H. Rokujo[c], O. Sato[c], T. Sato[k], H. Shibuya[l], K. Sugimura[c], L. Suzui[c], A. Suzuki[a], M. Suzuki[f], I. Usuda[c], S. Yamamoto[c], M. Yoshimoto[m],
(The NINJA Collaboration)

December 9, 2024

[a] *Kobe University, Kobe 657-8501, Japan*
[b] *Center of Excellence for Advanced Materials and Sensing Devices, Ruđer Bošković Institute, 10000 Zagreb, Croatia*
[c] *Nagoya University, Nagoya 464–8602, Japan*
[d] *Kyoto University, Kyoto 606-8502, Japan*
[e] *ICRR, The University of Tokyo, Kashiwa 277-8582, Japan*
[f] *Yokohama National University, Yokohama 240-8501, Japan*
[g] *Kavli IPMU (WPI), The University of Tokyo, Kashiwa 277-8583, Japan*
[h] *King's College London, London, WC2R 2LS, UK*
[i] *Nihon University, Narashino 275-8576, Japan*
[j] *Toho University, Funabashi 274-8510, Japan*
[k] *RCNP, Osaka University, Osaka 567-0047, Japan*
[l] *Kanagawa University, Yokohama 221-8686, Japan*
[m] *RIKEN, Wako 351-0198, Japan*

Abstract

The **NINJA** experiment stands for **N**eutrino **I**nteraction research with **N**uclear emulsion and **J**-PARC **A**ccelerator. It aims to conduct precise measurements of neutrino interactions in the Sub-Multi GeV energy range and to search for sterile neutrinos using an emulsion-counter hybrid detector with nuclear emulsion as the main detector and neutrino beams produced by the J-PARC accelerator. Thus far, the NINJA experiment has conducted proof-of-principle tests, test runs, and physics runs, using nuclear emulsion detectors with water and iron targets to measure neutrino interactions. We are now discussing the physics goals for the next decade and the means to achieve them.

This Letter of Intent (LOI) details several proposed objectives based on the results of previous experiments. These include: 1. Precision measurements of neutrino interactions using water-target nuclear emulsion detectors to provide crucial inputs for long-baseline neutrino oscillation experiments such as T2K, HK and ESSνSB, which uses large water Cherenkov detectors. 2. Measurements of neutrino-nucleon interactions using heavy water-target nuclear emulsion detectors, establishing a foundation for calculating all neutrino interactions. 3. Exploration of sterile neutrinos through high-statistics experiments using heavy targets, such as lead. This LOI presents these objectives in detail and outlines how they can be accomplished.

Keywords: NINJA, neutrino, cross-section, sterile neutrino, nuclear emulsion

*Corresponding authors: tfukuda@flab.phys.nagoya-u.ac.jp

Contents

1. Introduction

1.1. Physics motivation

Unmeasured properties of neutrinos, such as the leptonic CP-violating phase and neutrino mass ordering, represent key frontiers in particle physics. Their exploration through high-statistics neutrino oscillation experiments is underway worldwide. These experiments rely on nuclear targets to maximize statistics, using neutrino-nucleus ($\nu - A$) interaction models to reconstruct neutrino kinematics from the data. However, next-generation neutrino oscillation experiments face critical challenges due to systematic uncertainties in these models, which limit their precision and impact. Utilizing the emulsion cloud chamber detector (ECC), the NINJA experiment has already demonstrated its potential by collecting data in both neutrino and anti-neutrino modes (Sec. 1.2, Tab. 1). This effort has resulted in a series of cross-section measurement publications [1, 2, 3]. To further this work, we request an additional $\sim 1 \times 10^{21}$ protons-on-target (POT) exposure for the newly constructed ECCs, which may feature both water and heavy water targets.

Water Target Physics for Neutrino oscillations — At Tokai-2-Kamioka (T2K) [4] and Hyper-Kamiokande (HK) [5], beam neutrino oscillations are primarily measured through charged-current quasi-elastic (CCQE) interactions at energies below 1 GeV, where the observed final state typically consists of a single outgoing lepton. However, in nuclear media, these seemingly simple kinematics are altered by nucleon correlations, necessitating accurate models to control systematic errors. The high-resolution NINJA detector with a water target is well-suited to study these effects (Sec. 2, 3). Firstly, nuclear effects vary across targets, and using the same water target as T2K and HK far detectors eliminates potential biases. Secondly, observing outgoing nucleons is critical, as they provide direct insights into nuclear models. High-resolution detectors like NINJA can measure nucleon multiplicity and kinematics with precision, surpassing the capabilities of the T2K and HK near detectors. Current data in this area is sparse, so any additional inputs will significantly advance the field. These distributions will be made directly available to facilitate forward-folding comparisons with theoretical models, ensuring the utility of this water run despite the limitations in detector size and statistics.

Hadronic Final States for Neutrino Oscillations — Measuring neutrino mass ordering via neutrino oscillations requires detailed knowledge of hadronic final states. This is because experiments can access to inelasticity through hadron energy measurements which is an estimator of energy transfer, and this allows to charge separation and particle identification to boost the sensitivity of neutrino mass ordering [6]. For instance, HK relies on atmospheric neutrinos to measure neutrino mass ordering, where baryonic resonances (CCRES) and deep-inelastic scattering (CCDIS) dominate, making precise modelling of hadronic final states essential. Currently, data on final-state hadrons from neutrino interactions is scarce. NINJA's high-resolution detector can provide crucial information on hadron multiplicity and kinematics. Recent results from NINJA (T60, Run 6) [7] revealed an unexpected excess of backward-going pions (Fig. 1) suggesting a rich nature in hadron measurements with a high-resolution experiment such as NINJA. In addition to HK, water target experiments including ESSνSB [8], IceCube-Upgrade [9], and KM3NeT-ORCA [10] aim to use atmospheric neutrinos to measure mass ordering, highlighting the global demand for high-quality water-target neutrino beam experiments. NINJA's data will thus contribute significantly to worldwide neutrino oscillation programs.

Heavy Water Target and Axial Vector Form Factors — NINJA's water and heavy water targets provide a unique opportunity to study neutrino-nucleon interactions (Sec. 4), shedding light on the axial-vector response of nucleons—a fundamental property for understanding baryon structure. While vector current responses have been extensively studied from the photon and electron scattering, much less is known about the axial-vector response. This information is crucial for neutrino physics since vector-axial vector interference contributes to the differences between ν and $\bar{\nu}$ cross sections. Recent lattice QCD calculations of nucleon axial form factors [11] exhibit tensions with values from neutrino bubble chamber data traditionally used in neutrino oscillation experiments. The lack of a first-principle theoretical description of multi-particle systems such as $\nu - A$ interactions is yet possible, and these models need inputs of neutrino-nucleon data. NINJA's deuterium target will provide critical insights into axial vector form factors, a hot topic in both neutrino and nuclear physics. These results will also improve interaction systematics.

Other Advanced Nuclear Physics Topics — The axial current structure in the resonance region and beyond is even less understood. For example, the axial vector coupling of a nucleon to the Delta transition is somewhat measured for the I=3/2 channel, where $\Delta(1232)$ dominates the pion production amplitude. However, the contributions of non-resonance amplitudes and I=1/2 amplitudes, including their W-dependence, still need to be clarified. At higher

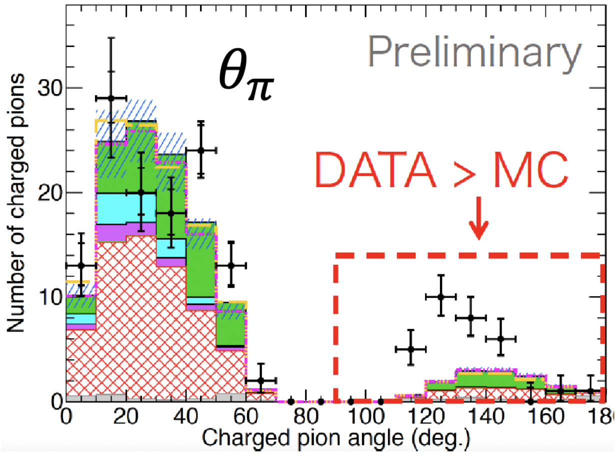

Figure 1: Preliminary result of charged pion angular distribution in NINJA anti-neutrino mode run (T60, Run6) [7].

energies, the axial current structure is even less understood. The so-called shallow-inelastic scattering region (the transition region from resonance to deep-inelastic scattering) is dominated by multi-meson production. The DCC model [12] accounts for the 2π channel and provides a satisfactory description of inclusive electron scattering. However, all reaction models may fail in this region for neutrino experiments due to the lack of knowledge of quark-hadron duality in the axial current. This region dominates reactions for low-energy neutrino telescopes, including IceCube-Upgrade [9] and KM3NeT-ORCA [10]. We expect NINJA can significantly contribute to these experiments, as well as to HK atmospheric neutrino measurements. NINJA is also valuable for exploring unmeasured processes and unknown hadron structures using neutrino beams. Recently, MicroBooNE succeeded in measuring Cabibbo-suppressed CCQE interactions in an argon target [13]. A high-resolution detector like NINJA is particularly useful for investigating rare topologies such as Λ and Σ^- productions. There is also speculation about enhanced pion production in antineutrino beams through the Λ production below the Δ production threshold [14]. This serves as an additional background for ν_e appearance searches and is worth exploring.

BSM Physics Topics — NINJA is an ideal experiment to uniquely explore certain types of beyond-the-standard-model (BSM) physics. The detector location can be optimized to maximize the sensitivity to sterile neutrinos (Sec. 5). Furthermore, high-resolution detectors are traditionally effective for investigating rare processes, both within the Standard Model and the BSM physics. This is evident from recent successes in high-resolution detectors including MicroBooNE [15]and CCM [16]. NINJA has a unique opportunity to search for new particles using a water target. The higher spatial resolution of the emulsion detector compared to liquid argon time projection chambers allows for NINJA to access topologies that are otherwise difficult to observe. Research in this exciting field has only just begun, and NINJA is positioned to make important contributions.

1.2. NINJA experiment

1.2.1. Nuclear emulsion

Nuclear emulsion has an intrinsic spatial resolution better than 1 μm in three dimensions and a comparable multi-track separation, as illustrated in Fig. 2 and Fig. 3. Therefore it is particularly suited for observing short-path decays, and also for disentangling events with multiple tracks. An emulsion film has two thin emulsion layers coated on both sides of a transparent plastic base, making up a micro-detector element of track position and angles. The main detector, designed as an Emulsion Cloud Chamber (ECC), consists of emulsion films interleaved with metal plates. Various material plates can be used in the ECC, which means that various target materials can be chosen to study neutrino-nucleus interactions [2]. Furthermore, by inserting nuclear emulsion films with some spacing in a water tank, it is also possible to conduct an experiment to study neutrino-water interactions [1]. Our ECC detector design, which is based on a sandwich structure of emulsion films and other material layers, enables us to detect low-momentum hadron tracks emitted from a neutrino-nucleus interaction separately and measure the emission angles of each track [3]. It

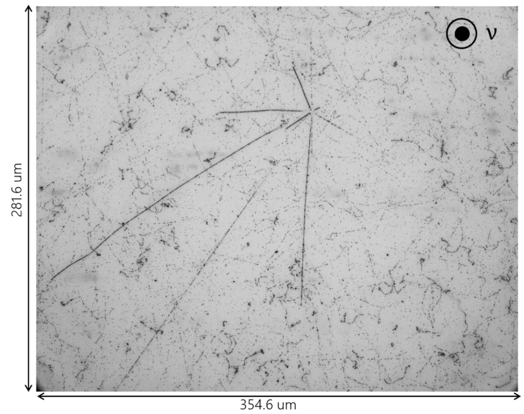

Figure 2: A Zoom-in to one emulsion film showing an example ν-iron interaction as observed in NINJA.

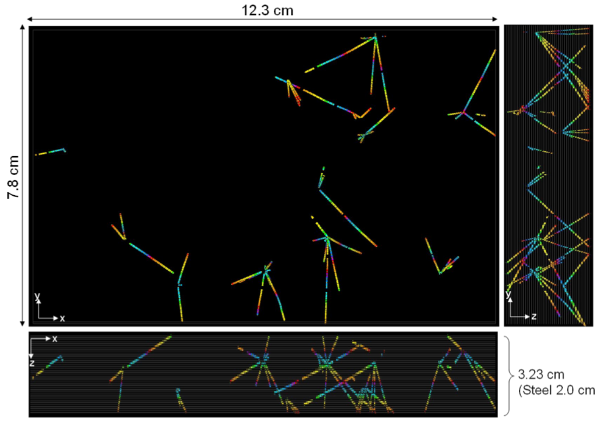

Figure 3: Reconstructed neutrino interactions in NINJA combining the recorded trajectories in a stack of emulsion films [17].

is possible to estimate the momentum of the hadrons from the measurements of multiple scattering in the material layer [18]. In NINJA, this can be used to achieve demonstrated momentum resolutions of 25-30% for muons, pions and protons [3]. Alternatively, when the tracks are contained in the detector, such as in the case of most low momentum protons, a range-energy relation can be used, capable of achieving excellent resolutions of 6% for muons, and 4% for protons [3]. By combining this momentum value with the ionization-loss value such as grain density and the pulse height measured in the detector [19], particle identification also becomes possible, as presented in Fig. 4.
As described above, the emulsion detector has many excellent features, there is however no time information in the emulsion detector itself because it is a storage-type detector with no dead time. To solve this problem, an emulsion shifter and a scintillation fibre detector are installed to add the time information to each track measured in the emulsion detector [20]. With matching the track information from the downstream electronic muon detector, each reconstructed vertex is analysed as a whole piece of the information on the neutrino-nucleus reaction.

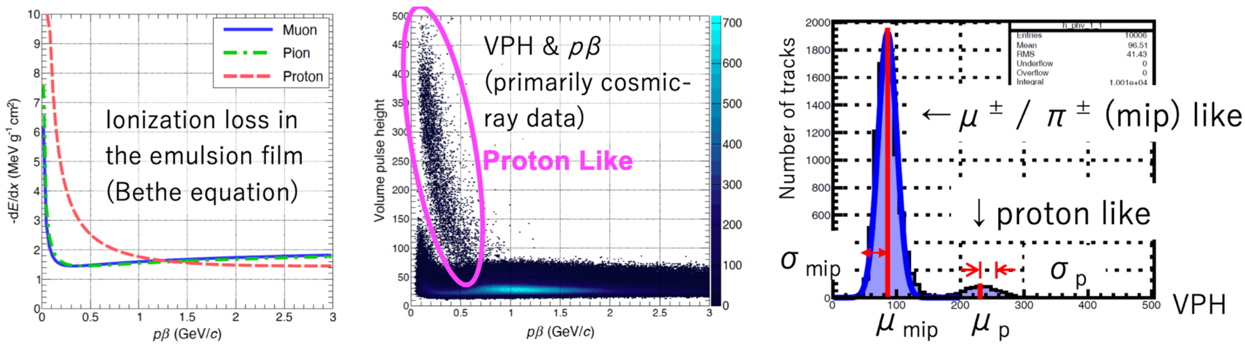

Figure 4: Left: Expected energy loss per unit length ($\mathrm{d}E/\mathrm{d}x$) for different particle types as a function of their momenta. Middle: The volume pulse height (VPH) measured in NINJA is directly indicative of the particle $\mathrm{d}E/\mathrm{d}x$. Right: VPH-based particle identification (PID) capabilities of NINJA, showing excellent capabilities to separate protons from muons and pions, often referred to as minimum ionizing particles (MIPs).

In order to achieve this, it is necessary to scan many emulsion films. In the past, readout of particle tracks in the emulsion was a time-consuming process. With the development of fully automated high-speed track-reading system and its continuous improvements and refinements, it has now become possible to obtain large amounts of track data quickly, including large-angle tracks up to $\theta \approx 80^\circ$, where θ is the track angle with respect to the perpendicular of the emulsion film (the beam direction) [21].

1.2.2. Past exposures

In 2014, we proposed a test experiment to develop a new emulsion-based neutrino detector at the near detector hall of the J-PARC neutrino beam line. Its physics aim was to study all the neutrino-nucleus interactions ($\nu_\mu/\overline{\nu_\mu}$-nucleus, $\nu_e/\overline{\nu_e}$-nucleus,) with high efficiency (with less bias), to detect hadrons emitted from the interactions with a low momentum threshold, and to measure their cross sections separately [22]. In the following years, we conducted a series of test experiments, T60, T66, and T68, in which we developed new ECCs, water-target systems, emulsion multi-stage shifters, and scintillating fiber trackers (SFT), etc. From these experiments, we had several technical demonstrations [17, 20] and obtained physics results on neutrino-iron interactions [2, 3] and neutrino-water interactions [1] although the statistics were limited. Then we carried out data-taking runs with a 75-kg water target as first physics runs, E71a and E71b. As shown in Fig. 5., a water-target ECC (Emulsion Chamber Counter) was used, consisting of a tracking unit made of two nuclear emulsion films sandwiched between a thin stainless steel plate and placed in a light-shielding bag, alternating with approximately 60 layers of water target sections in E71. Additionally, a Large Emulsion Shifter (LES) and a Scintillation Tracker (ST) [23] were installed behind the ECCs to provide time information for the neutrino interactions detected in the ECC, enabling the identification of muons with a downstream Muon Range Detector. The table 1 summarizes these exposures and data-taking runs for the NINJA experiment.

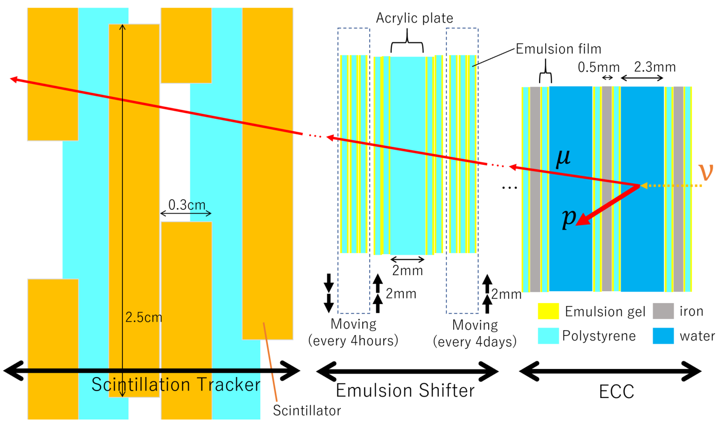

Figure 5: Detectors for E71

Table 1: History of the NINJA Experiment

Exp. Name	NINJA Run	Beam Period	Beam	POT ($\times 10^{20}$)	Taget and mass
T60	Run 1-3	Nov. 02, 2014 - Dec. 22, 2014	$\bar{\nu}$		Fe (2.0 kg)
	Run 4	Feb. 25, 2015 - Apr. 01, 2015	$\bar{\nu}$	1.4	Fe (2.0 kg)
	Run 5	May 08, 2015 - Jun. 03, 2015	$\bar{\nu}$	0.8	H_2O (1.0 kg)
	Run 6	Jan. 31, 2016 - May 27, 2016	ν	0.4	Fe (60 kg)
			$\bar{\nu}$	3.5	Fe (60 kg)
T66	Run 7	Jan. 31, 2017 - Apr. 12, 2017	ν	5.9	H_2O (1.3 kg)
T68	Run 8a	Oct. 14, 2017 - Dec. 22, 2017	$\bar{\nu}$	7.1	H_2O (3.0 kg)
	Run 8b	Mar. 09, 2018 - May 31, 2018	$\bar{\nu}$	in total	H_2O (3.0 kg)
E71a	Phys. Run 1a	Nov. 06, 2019 - Feb. 12, 2020	ν	4.8	H_2O (75 kg)/Fe (130 kg)
T81	Run 9	Feb. 26, 2021 - Mar. 26, 2021	ν	1.8	D_2O (9 kg)
E71b	Phys. Run 1b	Nov. 23, 2023 - Feb. 04, 2024	ν	3.1	H_2O (75 kg)/Fe (130 kg)
E71c	Phys. Run 1c	Nov. 2025 - (planned)	ν	≥ 2.1	H_2O (130 kg)/Fe (230 kg)

2. Water target run for T2K/HK experiment

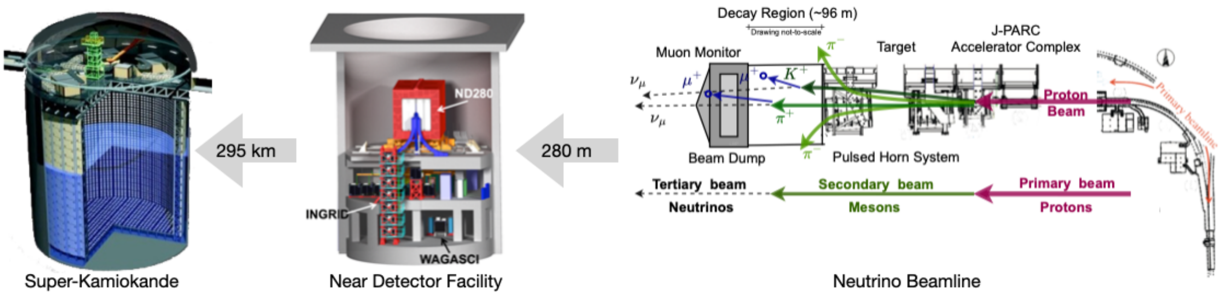

Figure 6: Layout of the T2K experiment, including the beam, its near detector facility at 280 m from the target, and the Super-Kamiokande detector 295 km further away. The HK experiment will utilize the same beam and near detector facility as T2K, and replace Super-Kamiokande with the HK detector, about eight times larger in size.

2.1. Introduction to Neutrino Oscillations

The three known neutrino flavors (ν_e, ν_μ, and ν_τ) are created in pure weak states but evolve into superpositions of mass states. This phenomenon leads to flavor oscillations –discovered two decades ago [24, 25]–, characterized by six parameters[26]: two mass-squared differences (Δm^2_{32} and Δm^2_{21}), three mixing angles (θ_{13}, θ_{23}, and θ_{12}), and one CP-violating phase (δ_{CP}). Here, m_1, m_2, and m_3 denote the neutrino mass states. In this landscape, three major unknowns remain: The sign of Δm^2_{32} (neutrino mass ordering), the conservation of CP symmetry (determined by δ_{CP}), and the octant of θ_{23} (whether it is smaller, larger, or equal to 45°) [27].
Deepening in our understanding of neutrino oscillations is of critical importance for contemporary fundamental physics. The lepton mixing pattern differs significantly from that of quarks. Resolving open challenges is paramount for unifying quark and lepton physics, revealing underlying symmetries [28, 29], and providing hints about the origin of the observed matter-antimatter asymmetry in the Universe [30, 4]. Precision neutrino oscillation measurements also have the potential of uncovering new physics effects, such as the existence of sterile neutrinos [31], later covered in Sec. 5, or non-standard neutrino interactions [32].

2.2. T2K and HK

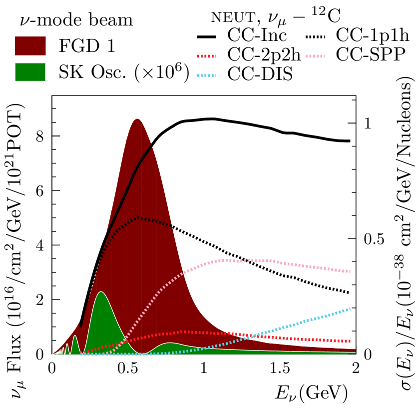

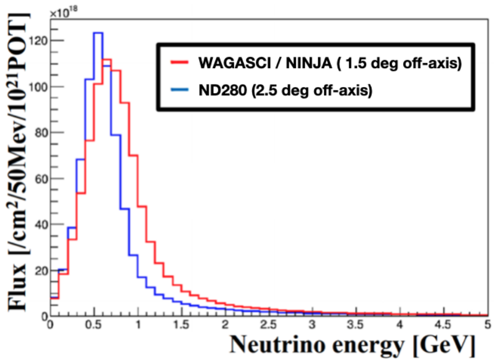

Figure 7: Left: Flux prediction at 2.5° off-axis at the near detector ND280 (FGD1 target) and far detector Super-Kamiokande. The size of the main cross section channels is also overlaid. Right: A direct comparison of the flux at ND280 vs that at WAGASCI and NINJA.

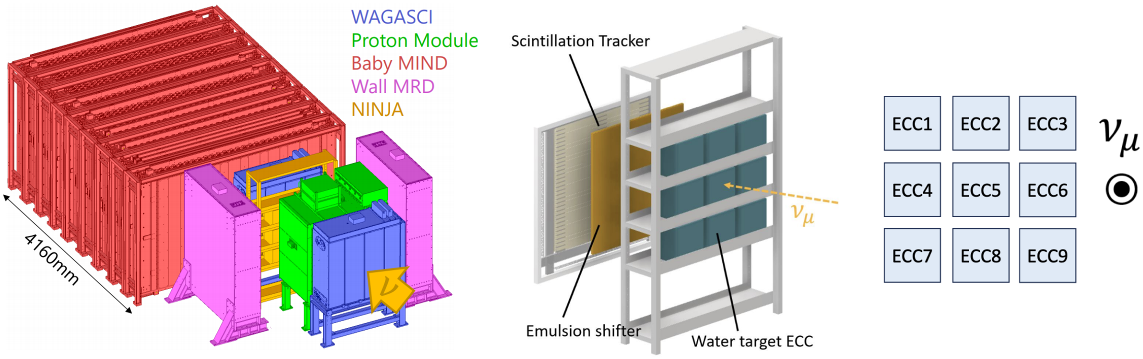

Figure 8: Left: A drawing of the WAGASCI-BabyMIND detector, including the placement of NINJA. Right: The configuration of NINJA in runs E71a, E71b. Including emulsion shifter to connect NINJA tracks to those in the other elements of WAGASCI-BabyMIND.

Among all existing experiments the leading sensitivity to Δm^2_{32}, θ_{23} and δ_{CP} is held by long-baseline (LBL) accelerator neutrino oscillation experiments. The T2K experiment [33], see Fig. 6, and the HK experiment [5], both in Japan, are respectively present and future world-leading LBL neutrino oscillations experiments. These experiments study the disappearance probability

$$P(\nu_\mu \to \nu_\mu) \approx 1 - 4\cos^2(\theta_{13})\sin^2(\theta_{23}) \times \left[1 - \cos^2(\theta_{13})\sin^2(\theta_{23})\right] \sin^2\left(\frac{1.27\Delta m^2_{32} L}{E}\right), \tag{1}$$

primarily sensitive to Δm^2_{32}, θ_{23}. Here L is the distance between the neutrino production and detection point and E is the neutrino energy. And the appearance probability:

$$P(\nu_\mu \to \nu_e) \approx \sin^2(2\theta_{13})\sin^2(\theta_{23})\sin^2\left(\frac{1.27\Delta m^2_{32} L}{E}\right) \mp \left(\frac{1.27\Delta m^2_{21} L}{E}\right) 8 J_{CP} \sin^2\left(\frac{1.27\Delta m^2_{32} L}{E}\right) \tag{2}$$

primarily sensitive CP-violating effects, encoded in the $\mp$ sign which is negative (positive) for (anti)neutrino oscillations. Here, J_{CP} is the so-called Jarlskog invariant [34, 35] $J_{CP} = \frac{1}{8}\cos(\theta_{13})\sin(2\theta_{12})\sin(2\theta_{23})\sin(2\theta_{13})\sin(\delta_{CP})$.
To precisely measure the oscillation probability, these experiments utilize three elements:

- Neutrino Beam: T2K utilizes a highly pure muon (anti)neutrino beam by focusing positive (negative) secondary mesons –typically pions– generated by colliding protons of the JPARC proton accelerator against a graphite target. Depending on the magnets' polarity a beam of neutrinos or antineutrinos is created, which is typically referred to as ν or $\bar{\nu}$ beam mode. The production yields of the secondary mesons and their propagation in the target are tuned using monitoring data at the JPARC facility in combination with external hadron production data of the NA61/SHINE experiment at CERN [36]. The JPARC neutrino beamline has recently been upgraded, enhancing its power from 0.5 MW to 0.8 MW. This major improvement is part of a longer upgrade plan [37], which is aimed at achieving 1.3 MW by 2027. In 2027, the HK experiment will start, inheriting the JPARC neutrino beamline from the T2K experiment. A particularity of T2K is that it uses to so-called off-axis beam technique, in which the detectors intentionally miss the beam center by a calculated amount to benefit from a modified neutrino energy spectra. Due to the pion decay kinematics, increasing off-axis translates into a smaller maximum energy, which translates into a narrow energy spectra, characteristic of T2K.
- Near Detectors (NDs): T2K's near detector facility has been evolving since the start of the experiment in 2010. Currently it consists of INGRID (0° off-axis), the near detector at 280 meters (ND280) (2.5° off-axis) and the WAGASCI-BabyMIND detector (1.5° off-axis). INGRID, features a cross-like shape is used to monitor the beam direction and intensity on a daily basis. ND280 is built up of multiple detector sub-modules featuring complementary technologies. ND280 original targets consist of FGD1 and FGD2 [38], consisting of layers of plastic scintillator bars oriented in alternate axis in consecutive layers. FGD1 is full plastic, while FGD2 replaces half of the detector mass layers of inactive water. In 2024 ND280 has been upgraded [39]

to include SuperFGD [40, 41], a new full plastic detector with 3D granularity. In addition, ND280 features gaseous time-projection-chambers [42] and an electromagnetic calorimeter, all within the UA1 dipole magnet, acting also as a side muon range detector [43]. In 2020 a new near detector WAGASCI-BabyMIND was installed, also consisting of several sub-module technologies, including WAGASCI [44], a new target concept with 3D granularity made up of 80% inactive water, and BabyMIND [45], a magnetized muon range detector. WAGASCI-BabyMIND, see Fig. 8 also hosts the NINJA detector. Due to its common technical aspects, including the beam modeling and the sharing of detector data, and its research synergies, presented later, NINJA and T2K experiments are currently actively collaborating and articulate the necessary data sharing and knowledge transfer via a dedicated working group, `T2K-NINJA` created in early 2024.

- Far Detector (FD): The far detector of T2K is Super-Kamiokande [46] (SK), the largest water Cherenkov detector in the world and one of the most important existing neutrino detectors. SK is placed 295 km away from the beam creation point, at 2.5° off-axis, same as the ND280 near detector. At 2.5° off-axis the neutrino energy peaks at 0.6 GeV, such that 295 km away, when the neutrino beam reaches SK, the oscillation probability from the muon flavor to the electron flavor, often referred to as $P(\nu_\mu \to \nu_e)$ is expected to be nearly maximal, producing a dramatic difference between the unoscillated and oscillated flux –presented in the left panel of Fig. 7– and allowing to perform precision neutrino oscillation studies. In 2027, the HK detector will start its operations, and the HK collaboration will inherit the beam and near detector facilities of T2K resulting in the long baseline accelerator physics program of HK (HK). The HK detector relies on the same well understood and highly successful detection technology of SK, but increases its fiducial mass by $\approx \times 8$. The size increase, paired with the increased beam power, will allow HK to collect beam neutrinos about 20 times faster than T2K in 2020, transforming the sensitivity of the experiment, which is currently limited by systematic uncertainties to a new scenario where the limit to the sensitivity are systematic uncertainties.

T2K in the present, and HK in the future, combine data at the two detector sites (NDs and FDs) together with external data (NA61/SHINE, in the future NINJA) to draw statistical conclusions on the neutrino mixing properties. This strategy has been already demonstrated as greatly successful, with T2K as one of the most influential experiments on the field of neutrino physics in the last decade. T2K measured the first indications of a non-null θ_{13} angle [47], is leading the measurement of the value of θ_{23} and Δm^2_{32} [48] and has provided the first strong indications[1] of CP-violation (strongly disfavoring CP-conserving values $\delta_{CP} \neq 0, \pi$) [4], a search that is among the most important studies in the scientific program of HK [5].

2.3. Research Challenges and the Need for Water Measurements

To study neutrino oscillations, see Eqs. 1 and. 2, identifying the neutrino flavor is crucial. Neutrino oscillation experiments do that by identifying the flavor of the final-state charge lepton produced by charged-current (CC) neutrino interactions. For instance, a CC ν_μ ($\bar{\nu}_\mu$) interaction will produce a μ^- (μ^+) particle, whereas a CC ν_e ($\bar{\nu}_e$) interaction will produce a e^- (e+) particle. At the operation energy of T2K experiments, i.e. neutrino energies around 1 GeV, the dominant interaction mode consists of neutrino-nucleon scattering, which can occur through several channels, see Fig. 7, including CC quasi-elastic (CCQE) $[\nu + n \to \mu^- + p]$, resonant (CCRES) $[\nu + p \to \mu^- + \pi^+ n]$ and deep-inelastic scattering (CCDIS) interactions [when the interaction happens with a quark, typically producing several final-state hadrons]. Since interactions happen with a nucleon bound in the nucleus (Carbon, Oxygen, etc), they are subject to a plethora of nuclear effects, illustrate in Fig. 9. For instance, interactions can happen with a heavily bound pair of nucleons (2p2h) by meson exchange current (MEC) and the final state particle kinematic distributions and particle contents are modified due to re-interactions experienced when escaping the dense nuclear medium, known as Final State Interactions (FSI). These nuclear effects have a significant impact when reconstructing the incident neutrino energy, as illustrated in Fig. 10, and therefore the study of neutrino-nucleus interactions is of critical importance in contemporary neutrino physics since better understanding them is key to enable further precise neutrino oscillation measurements.

T2K, and in the future HK, utilizes the capabilities of the far detector to split neutrino interactions according to its flavor (muon or electron) and the presence or not of a charged pion. However, water Cherenkov detectors are blind to low momentum protons –protons only produce a significant amount of Cherenkov light above 2 GeV/c–, which are

[1]The result was highlighted as one of the top 10 remarkable discoveries of the year by the journal Nature [49].

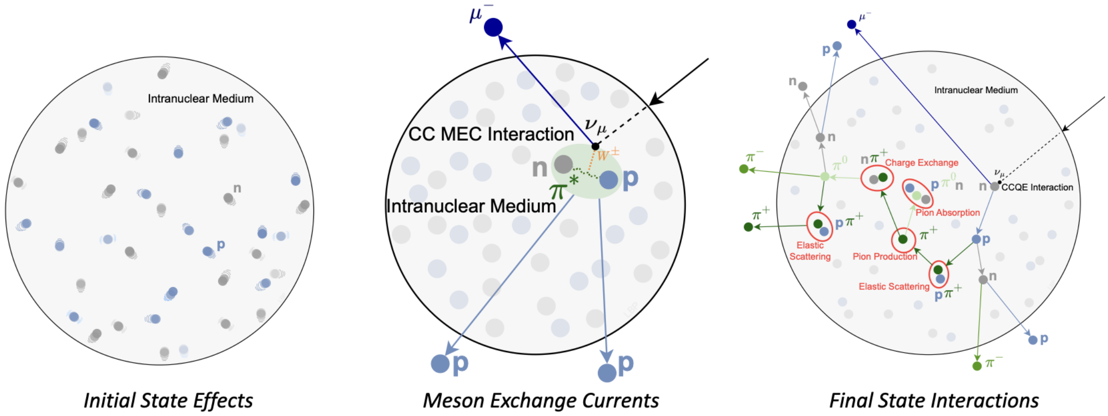

Figure 9: Illustrations of several nuclear effects affecting the reconstruction of the incident neutrino properties. Left: The initial nucleon is not free nor stationary, but instead is moving with an initial momentum distribution and bound to nucleus with a certain binding energy. Center: Some nucleons are very strongly bound to one-another via so-called meson exchange currents, responsible for multi-nucleon knockout in which the incident neutrino effectively strikes several of these highly bound nucleons. Right: The final-state particles are created in a dense nuclear medium and therefore are subject to interactions that can transform the particle content or types (charge exchange, pion absorption, proton absorption, de-excitation, etc) and kinematics (e.g. via scattering). Image credit: Ref. [50].

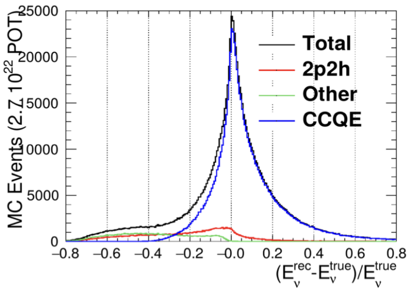

Figure 10: Neutrino energy reconstruction in T2K exploiting four momentum conservation and assuming a true CCQE interaction with an initial stationary nucleon for several interaction channels.

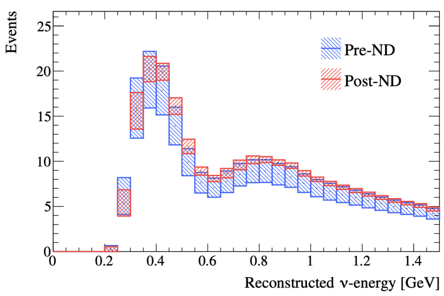

Figure 11: Predicted event rate spectra in SK for ν_μ CCQE-like events in SK (1μring sample), before and after the near detector flux and cross section model constraint.). Plot from Ref [48].

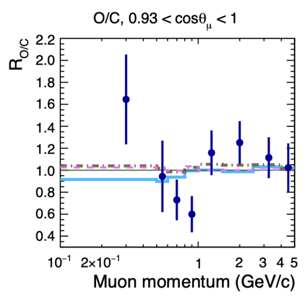

Figure 12: Expected and measured Oxygen vs Carbon cross section ratio (R_{OC}) in the forward muon region. Plot from Ref [51].

of great importance. For instance, events with a single final state proton and no pions correspond typically to a true CCQE event, whereas the presence of multiple protons (e.g. 2p2h) is symptomatic of the presence of significant nuclear effects (e.g. MEC). Since SK can not quantify the fraction of events experiencing these effects, T2K relies on its near detectors, primarily ND280, to quantify these effects and assess what model prediction variations are statistically consistent with the recorded data. The near detector data constraint, which also allows to tune the nominal flux prediction, is of critical importance for T2K, see in Fig. 11, enabling its leading sensitivity to neutrino oscillation physics.

Error source	ν_e **1R**	ν_μ **1R**	$\bar{\nu}_e$ **1R**	$\bar{\nu}_\mu$ **1R**	ν_e **1R d.e.**	ν_μ **CC1**π
T2K 2022 POT [targets FGD1+FGD2]						
Flux+Xsec (ND constr)	4.1%	3.8%	3.7%	3.6%	5.0%	3.5%
Upgraded T2K 2027 POT [targets FGD1+FGD2+SFGD]						
Flux+Xsec (ND constr)	2.7%	2.5%	2.3%	2.3%	3.1%	2.4%
Upgraded T2K 2027 POT including 100% C/O correlation [targets FGD1+FGD2+SFGD]						
Flux+Xsec (ND constr)	1.8%	1.7%	1.8%	1.7%	1.9%	1.5%

Table 2: Systematic uncertainties in the six Super-Kamiokande samples in percentage for T2K pre-upgrade (2022), post-upgrade (2027), and post-upgrade but including 100% systematic error correlations for Carbon and Oxygen parameters [52].

The goals of the T2K experiment have changed significantly since its start in 2010. At that time θ_{13} was not known to be non-zero, a necessary requirement to measure CP-violation in neutrino oscillations, as it is explicit in Eq. 2. Similarly, much progress has been made in the last decade in understanding the role and magnitude of several nuclear effects affecting neutrino-nucleus interactions. This combined progress has been an important ingredient in the decisions of the ND280 detector upgrade completed in 2024, the installation of a new near detector, WAGASCI-BabyMIND in 2019, and the design of the HK experiment, which will include an additional intermediate water Cherenkov detector (IWCD) at about 1 km from the neutrino production point. The goals of these upgrades are as follows. The ND280 upgrade, featuring the new SFGD target, will enable a much further detailed understanding of nuclear effects in Carbon, thanks to a much lower tracking threshold than previous ND280 targets, thus providing invaluable datasets for theorists to refine and validate existing models and for T2K and HK to constrain their predictions, as earlier exemplified in Fig. 11, with the goal of enhancing its existing sensitivity. The one caveat of the ND280 upgrade, however, is that it studies neutrino-Carbon interactions, whereas water Cherenkov detectors such as SK and HK, are made of water (H_2O). Therefore, there is a limit on how much one can constrain existing uncertainties unless unless it is possible to extrapolate precise data on Carbon to Oxygen constraints. To do exactly that, ND280 has a target with some water on it, named FGD2, which is of great help for that task, and has been used in the past to study C vs O differences, which are known to be significant for those events where the final-state muon is very forward, see Fig. 12. Despite of the critical role of FGD2, and as presented in Tab. 2, T2K and HK would greatly benefit from additional data on water which would allow to more strongly correlate uncertainties for interactions in Carbon and Oxygen. Recognizing the importance of having further data on water, the WAGASCI-BabyMIND detector was installed, featuring both a 100% plastic (CH) target (Proton Module) and a hybrid water (80%) plastic (20%) targets (WAGASCI). This addition will double the statistics in water for T2K, and will allow to disentangle degeneracies in cross section and flux parameters by doing measurements at a slightly different off-axis, earlier presented in Fig. 7. HK, will further benefit from additional data on water utilizing IWCD, featuring the same detection method as HK. There is, however, a fundamental limitation. Both FGD2 and WAGASCI have high hadron detection thresholds, similar to 450 MeV/c for protons. In IWCD, this threshold is even larger, at around 2 GeV/c. Therefore, although existing and planned T2K and HK detectors can study interactions in water, their constraints are strongly limited to a description of the leptonic part of the interaction (i.e. a description of the final state lepton kinematics). If one could, in addition, have a strong direct constraint of the hadronic part of the interaction, powered by precision measurements of final-state low momentum protons and pions in water, this would enable a much more reliable energy reconstruction for the incident neutrinos, which would dramatically boost the sensitivity of T2K and HK to neutrino oscillations.

	CCQE-1p1h	CCQE-2p2h	CCRes-1π	CCDIS multi-π	CC-Other
All Events	6710.0	1347.1	6078.8	2822.7	317.9
Selected Events	1169.8	300.2	1216.4	830.2	99.8

Table 3: Expected events in NINJA according to NEUT v5.7.0 per every 100 kg of water and 1×10^{21}. The total number of events and the expected number of selected events after requiring a reconstructed muon track in BabyMIND are presented.

2.4. Understanding neutrino-water interactions with NINJA

NINJA has all necessary characteristics for an ideal near detector for T2K and HK. It pairs excellent particle identification capabilities with exceptional tracking granularity, enabling detailed studies of neutrino interactions in water. Thanks to those capabilities NINJA has the potential to drastically transform the modern knowledge on neutrino nucleus interactions while releasing data and measurements that would be immediately beneficial for T2K and HK. A list of pioneering measurements that would be enabled by high event rates in NINJA include. Expected event rates for different reaction types for every 100 kg of water and 10^{21} POT are summarized in Tab. 3.

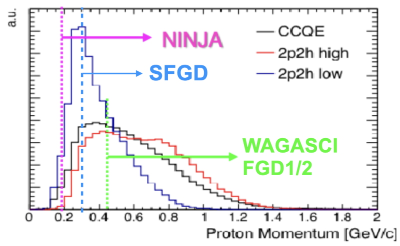

Figure 13: Expected proton momentum distribution for different interaction modes (CCQE, 2p2h) compared to the detection thresholds of FGD1 and WAGASCI T2K targets and NINJA. In the case of 2p2h the momentum of both the highest (high) and lowest (low) momentum proton is presented.

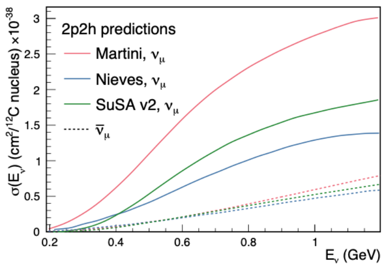

Figure 14: Cross-section predictions for ν_μ (solid) and $\bar{\nu}_\mu$ (dashed) 2p2h interactions on ^{12}C from Martini et al. [53], Nieves et al. [54], and SuSA v2 [55, 56]. Reproduced from Ref. [48].

• **Precision studies of multi-nucleon knockout in water.** The high granularity of NINJA enables precision measurements of the proton production yields and their kinematic distributions. There is significant theoretical literature on the topic [53, 57, 58, 54, 55, 56, 59, 60, 61, 62], but data is generally extremely scarce, and inexistent for water. The 200 MeV/c proton tracking threshold implies that NINJA is sensitive to practically the totally of all protons momenta in neutrino-nucleus interactions. NINJA is not only capable of studying this interactions in water, but its tracking capabilities make it unmatched when compared to targets of any other experiment, including T2K, as presented in Fig. 13. As presented in Tab 3 NINJA expects hundreds of 2p2h interactions, allowing to perform detailed studies on the process. These measurements are critical to validate and enhance existing model predictions, which are widely different, as presented in Fig. 14. The capabilities of NINJA would enable to go even one step further, performing a first measurement of 3p3h, which is expected to be around 10-20% of 2p2h. Most modern neutrino interaction generators do not include 3p3h in their predictions.

• **Detailed characterization of FSI in water.** Pion FSI is of great importance, for instance, the absorption of the charged pion in a CC-RES event can induce the same final-state particle content of a CCQE interaction. Currently, both T2K using beam neutrinos and Super-Kamiokande using atmospheric neutrinos are observing a significant excess of low momentum pions associated with events with low momentum final-state leptons, as presented in Fig. 15. This excess could be explained by a significant mis-modeling of pion FSI. T2K, using the ND280 detector, has made a recent measurement in Cabron using FGD1, and, no excess has been observed [64]. However, NINJA –even if with low statistics– observed a strong absence of events with a single pion in water, as presented in Fig. 16. Therefore, to elucidate this tension is therefore imperative to do the measurement in water, where FSI might be significantly different. As presented in Tab. 3, NINJA can collect a large number of events with and without pions in the final-state, essential for this measurement. To characterize pion FSI, NINJA can measure so-called transverse kinematic imbal-

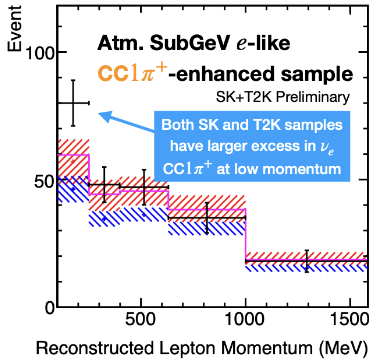

Figure 15: Observed data and predictions with 1σ uncertainties show significant excess for CC events with pions (CC$1\pi^+$) both in T2K beam and SK atmoshperics data. Ref [63].

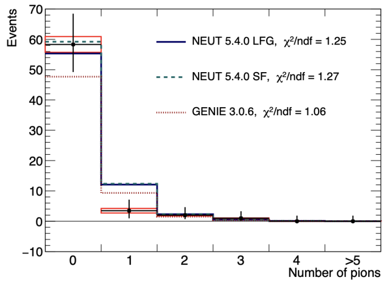

Figure 16: Expected pion multiplicities in water according to NEUT 5.4.0 compared to NINJA measurements. Figure reproduced from Ref. [1].

ance (TKI) variables, very sensitive to these effects. In TKI, one projects the measured track's kinematic variables in the plane that is most informative to nuclear effects. Examples of this variables include:

$$\delta\vec{p}_T = \delta\vec{p}_T^{\mu} + \delta\vec{p}_T^{\pi} + \delta\vec{p}_T^{p} \tag{3}$$

$$\delta\alpha_T = \arccos\frac{-\delta\vec{p}_T^{\mu}\cdot\delta\vec{p}_T}{\delta^{\mu} p_T \delta p_T} \tag{4}$$

$$p_N = \sqrt{\delta^2 p_T + \delta^2 p_L} \tag{5}$$

which can be applied also to pionless events by simply removing the $\delta\vec{p}_T^{\pi}$ contribution, and double-transverse momentum imbalance variables:

$$\delta p_{TT} = \delta p_{TT}^{\pi} + \delta p_{TT}^{p} \tag{6}$$

$$\delta p_{TT}^{\pi} = \vec{p}_{\pi}\cdot\hat{z}_{TT} \equiv \vec{p}_{\pi}\cdot\frac{\vec{p}_{\nu}\times\vec{p}_{\mu}}{|\vec{p}_{\nu}\times\vec{p}_{\mu}|} \tag{7}$$

$$\delta p_{TT}^{p} = \vec{p}_{p}\cdot\hat{z}_{TT} \equiv \vec{p}_{p}\cdot\frac{\vec{p}_{\nu}\times\vec{p}_{\mu}}{|\vec{p}_{\nu}\times\vec{p}_{\mu}|} \tag{8}$$

These variables have shown significant disagreement with data, both for events without [65] and with pions [66]. The disagreement is particularly strong for pionless events in regions with large $\delta\alpha_T$ and δp_T, and for events with pions with the large δp_{TT}, examples for each are presented respectively in Fig. 17 and Fig. 18. Those regions associated to events strongly influenced by nuclear effects. Existing TKI measurements are limited to plastic and Argon targets, without any data on water further strengthening the importance of NINJA's data.

• **Understanding the production yields of nuclear fragments.** When particles experience nuclear FSI, energy is transferred to the nucleus, which can then break or re-adjust by emitting nuclear fragments via de-excitation. The emitted fragments, such as deuterium (D), tritium (T), 3He and α particles, is widely different in existing models, see Fig. 19. The final-state fragments are expected to be low momentum and very ionizing, such that only a detector with exceptional tracking and ionization capabilities like NINJA can do this measurement. Such data, reported for instance as expected versus observed production yield for different nuclear models, would be invaluable to advance the current modeling of FSI and include a correct treatment of nuclear de-excitation which would otherwise bias the measurements of detectors relying on the visible energy as a proxy for the hadronic activity in the system.

• **Precision measurements of CCQE interactions in the forward region.** Pionless interactions are known to be in disagreement with existing neutrino-nucleus scattering data in T2K [71, 51] and MINERνA [72, 73], particularly in regions of low momentum transfer (Q^2). T2K used to deal with this via the inclusion of a nuclear screening

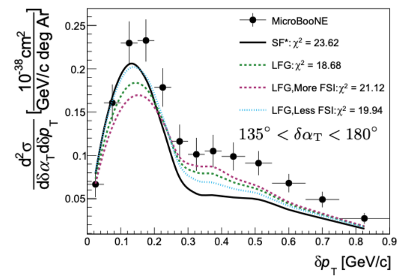

Figure 17: MicroBooNE results compared with predictions using the NEUT LFG model. The effects of adjusting the nucleon mean free path by -(+)30% are displayed and labeled as *More(Less) FSI*. Figure reproduced from Ref. [65].

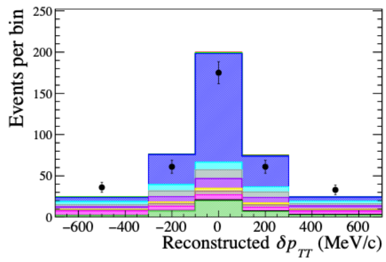

Figure 18: Measured vs expected events in the FGD1 plastic target of T2K as a function of δp_{TT}. Figure reproduced from Ref. [66].

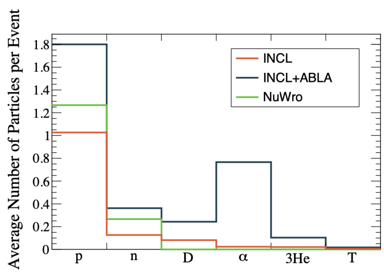

Figure 19: Average number of particles produced per event for INCL [67], INCL coupled with ABLA [68] and NuWro [69]. NuWro produces only protons and neutrons. Figure reproduced from Ref. [70].

effect using the Random Phase Approximation (RPA) [54]. However, in order to account for nuclear shells, T2K is now describing the nuclear initial state via a Spectral Function (SF) [74], which strongly relies on the impulse approximation, i.e. the assumption that the initial nucleon is at rest, which is expected to break down at low momentum $Q^2 \lesssim 400$ MeV/c [75]. To deal with this limitation T2K introduces an *ad hoc* Q^2-dependent parametrization to perform a data-driven tune of the baseline prediction for low-Q^2 values [48]. Data of NINJA is particularly well suited to investigate neutrino-nucleus interactions for this events for low-Q^2 events, which can then be used to assess the validity of T2K's parametrization and constrain the size of its prior uncertainties increasing T2K sensitivity.

• **Inclusion in the near detector fitting.** In the T2K experiment, the near-detector data are fitted with the MC prediction to give constrains on the neutrino flux and cross-section systematic errors. One possible approach is to include the NINJA data to the fit along with the T2K near detector. We performed a sensitivity study with simulated NINJA and T2K data with 2×10^{21} POT and 20×10^{21} POT, respectively[76]. Figure 20 shows the error size of the cross-section systematic parameters before and after the fitting. Although errors of some parameters, especially the 2p2h parameters, are reduced by including the NINJA data in the fit, its effect is limited. As a result, even if the fitting including NINJA is used in the oscillation analysis, confidence regions of the oscillation parameters will not be significantly changed as shown in Fig. 21. It may be because the T2K neutrino oscillation models and parameters are optimized for the fitting with the T2K detectors. It is newly optimized considering the NINJA detector, the inclusion of the NINJA data will have bigger impacts on the T2K oscillation results.

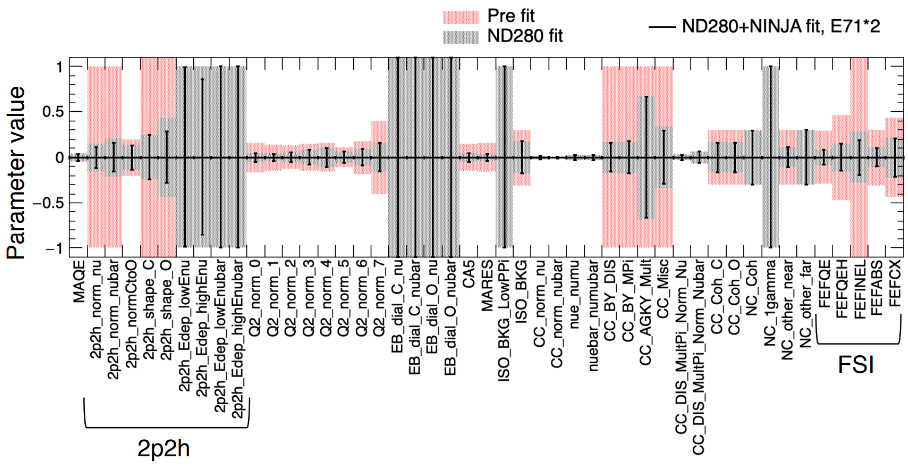

Figure 20: Error size of the cross section systematic parameters before and after the near detector fitting including NINJA.

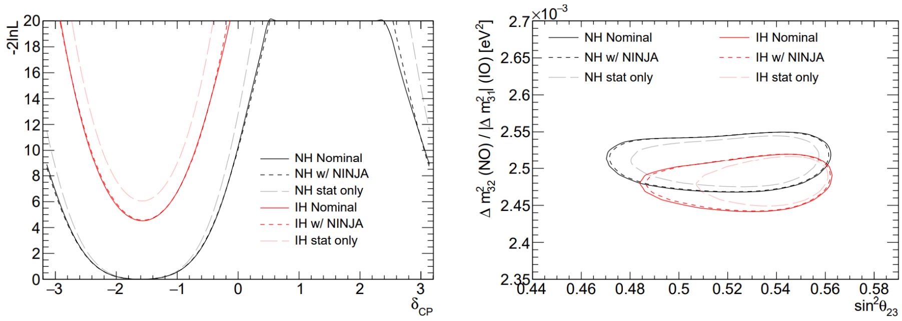

Figure 21: Contours of the 68% confidence level of $\sin^2\theta_{23}$-$|\Delta m^2_{32}|$ and negative log-likelihoods of δ_{CP} calculated with constraints on θ_{13} from reactor experiments.

2.5. *Experimental setup*

The baseline plan is running an experiment in the same or similar detector setup as E71 in the B2 floor (Fig. 22). We use water target ECCs. They are made of sandwich structure of emulsion films and water target as well as iron plates used for the momentum reconstruction using multiple Coulomb scatterings. An emulsion shifter and a scintillator tracker are used to give a timing information to tracks recorded in the ECCs. We are now developing a new emulsion shifter and a new scintillator tracker for the next physics run planned in 2025 which cover wide area of the ECCs with a better positional resolution. The BabyMIND detector which is a part of the T2K detector is located in the downstream of the ECCs and it is used as the muon range detector. The T2K experiment will operate and analyze BabyMIND until 2026 and provide the analyzed data to NINJA following an MoU between T2K and NINJA. However, the operation plan of BabyMIND beyond 2027 is not yet decided. We request J-PARC to keep the BabyMIND detector in B2 floor for this running option. In this running option, we can reuse a large part of the detectors and analysis methods developed for E71. In addition, we can combine the new data with E71 data to gain statistics in the analysis. The 4×4 ECC configuration gives 133 kg water target mass. When the J-PARC Main Ring power is increased to 1 MW, 1×10^{21} POT is expected in three month beam operation.

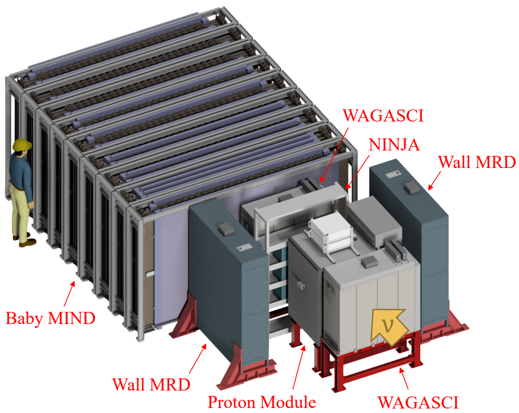

Figure 22: Detector setup of E71

One possible modification to the setup in E71 is tilting the ECCs. In E71, ECCs are installed so that the emulsion films in the ECCs are perpendicular to the neutrino beam. As a result, the ECCs are not sensitive to particles scattered in 90° to the beam and we could not measure continuous angular distributions from 0 to 180° as shown in Fig. 23. If we tilt the ECCs as shown in Fig. 24, we can detect particles scattered in 90°. By combining the data of the tilted ECCs with normal ECCs, we can measure the continuous angular distribution from 0 to 180°.

2.6. *Summary*

We propose a neutrino-nucleus interaction experiment using J-PARC's neutrino beamline, directly benefiting T2K and HK experiments. The NINJA detector's proven exceptional tracking of low-energy particles enables unprecedented precision in studying nuclear effects. This capability will allow first-time precision measurements of multi-nucleon knockout in water, investigation of T2K and SK tensions regarding low-energy pion production, and pioneering measurements of nuclear fragment yields to understand de-excitation and final-state interactions. These results will help validate theoretical models and constrain experimental uncertainties, particularly in establishing correlations between neutrino-Carbon and neutrino-Oxygen interactions, critical for improving neutrino oscillation measurements and enhancing their sensitivity.

The baseline experimental setup is the same as that in E71. We will place ECCs, an emulsion shifter, and a scintillator tracker upstream of BabyMIND. The BabyMIND detector which is part of the T2K detector will be used as a muon range detector. One possible modification to the E71 setup is tilting the ECCs to give sensitivity to particles scattered 90° to the beam. We will decide on the optimal detector setup based on the sensitivity study.

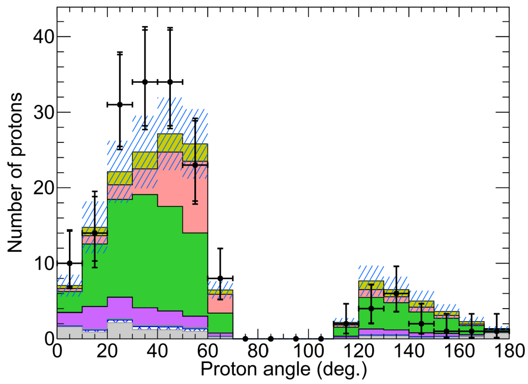

Figure 23: Reconstructed proton angle distribution measured by the NINJA experiment.

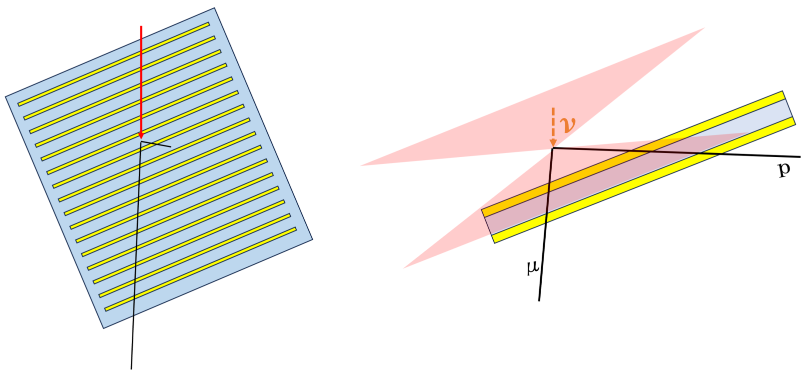

Figure 24: Tilted ECC with respect to the neutrino beam.

3. Water target run for ESSνSB project

3.1. Physics motivation

The ESSνSB project [77, 78] is a design study for a next-to-next generation neutrino oscillation experiment to very precisely measure the amplitude of the CP violation in the leptonic sector. It is foreseen to run after HK [5] and/or DUNE [79] have already confirmed (or excluded) the existence of the CP violation. ESSνSB will measure neutrino oscillations in both the first and the second oscillation maximum, significantly reducing the effect of systematic uncertainty on the precision of CP amplitude measurement. The far detectors will be placed 360 km away from the source and will consist of two large water Cherenkov detectors with a total fiducial water mass of 540 kt. The energy range of the ESSνSB muon neutrino beam will be roughly 60-600 MeV. The current data on (anti)neutrino interaction cross-sections in this range, especially below 400 MeV, is very scarce or nonexistent (see Fig. 25). This energy region is also expected to have a significant contribution from meson-exchange-current (MEC) interactions which pose a background to experiments relying on measurements of quasi-elastic neutrino scattering. The run proposed in this section would be the first measurement of the neutrino cross-section in this interesting energy region.

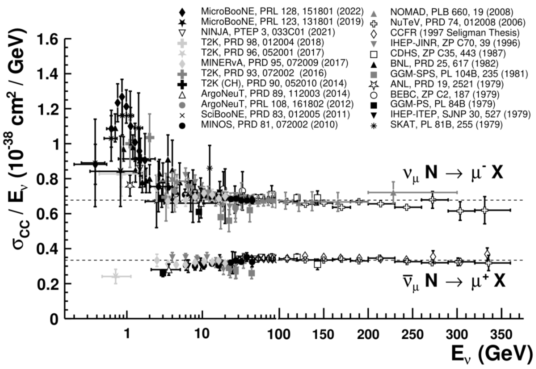

Figure 25: Overview of current measurements of the inclusive ν_μ and $\bar{\nu}_\mu$ CC interaction cross-section divided by neutrino energy. Note the scarcity of data for neutrinos and a complete lack of data for antineutrinos below 400 MeV. Reprinted from [80].

3.2. Neutrino flux and expected interaction properties

To reach the 60-600 MeV energy band, it will be necessary to measure at a very large off-axis angle w.r.t. the center of the T2K beam which peaks at about 1 GeV. The candidate site is the ground level of the NM building at J-PARC and the surrounding area. For the purposes of this LOI, two placements of the detector were considered: the center of the ground level of the NM building and a point outside toward the NA building. The muon neutrino fluxes and corresponding charged-current (CC) interaction rates are shown in the Fig. 26. Interaction rates were computed assuming 500 kg water target and CC interaction cross sections provided by GENIE [81, 82, 83] neutrino event generator (version 3.4.2 and tune G18_02a_00_000).

From Fig. 26 it is visible that outside of the NM building the main peak of the ν_μ flux is too low for the purpose of this measurement, as it is below the muon production threshold; the peak is not present at all in the event rate spectrum. On the other hand, in the center of the NM building the ν_μ flux peaks at higher energies, which results in a prominent peak around 400 MeV in the expected event rate. Therefore, the positioning of the detector outside of the NM building will not be considered further.

The comparison of the expected ν_μ CC event rate beam at the NM building and the one at the ESSνSB near detector site is shown in Fig. 27. It can be seen that the overlap at the sub-GeV region is remarkably good, but the NM spectrum has in addition a high-energy tail. An algorithm will need to be devised to select the events in the sub-GeV region of interest.

To further study the flux at the ground level of the NM building, expected CC interaction rates have been calculated for all flavor components of the T2K beam. These spectra are shown in the Fig. 26. As expected, the main contribution to the CC interactions comes from the ν_μ component of the beam, while the contribution of the other flavors are of

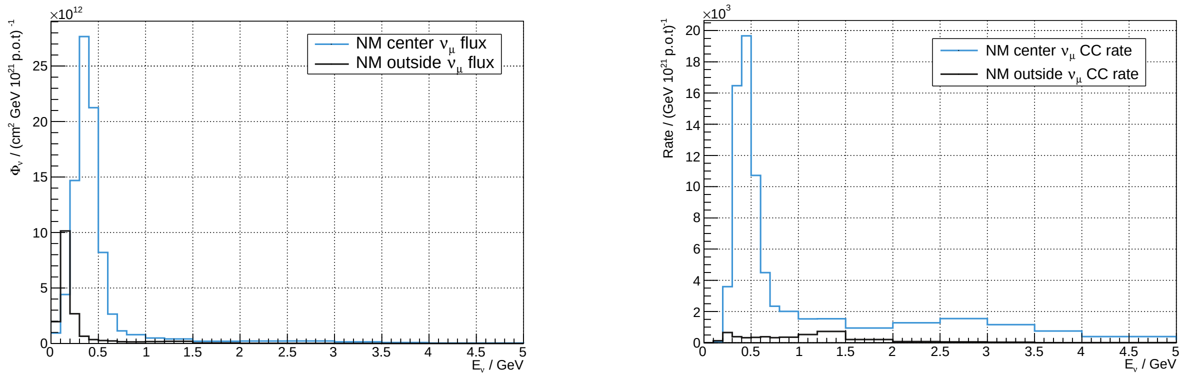

((a)) Neutrino flux

((b)) Interaction rate assuming 500 kg target mass and 10^{21} p.o.t.

Figure 26: Expected ν_μ flux and CC interaction rate compared for the two detector placements: center of the ground floor of the NM (blue) building and outside of the NM building (black).

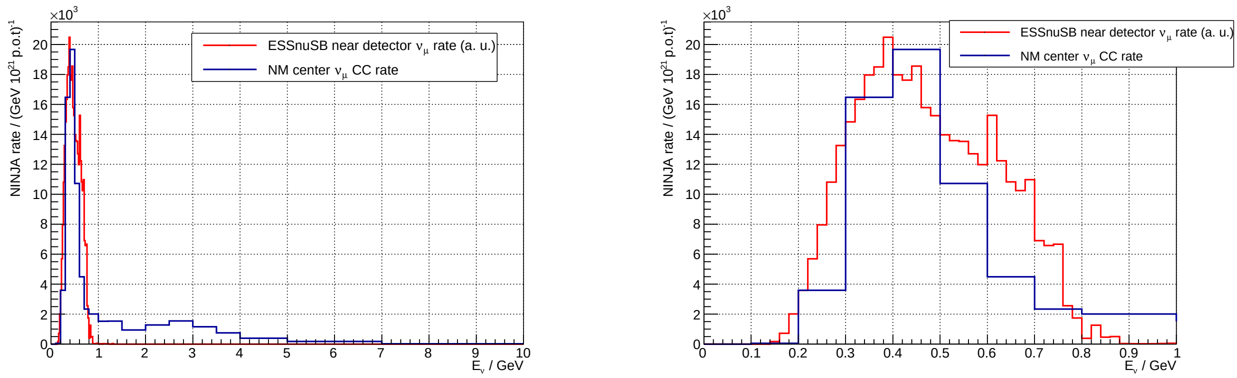

((a)) Full energy range

((b)) Zoom to the sub-GeV range

Figure 27: Expected ν_μ interaction rate at the NM ground floor (blue) compared the one at the ESSνSB near detector (red). The ESSνSB rate is not normalized.

the sub-leading order. Nevertheless, their contribution as a possible source of background will be studied in the experiment proposal.

The total number of expected interactions, both CC and NC, are shown in the Table 4. The pion-producing NC interactions might constitute background for the ν_μ CC measurement. It is expected that about 23% ν NC interactions will have a charged pion in the final state, corresponding to about 1100 such events which is about 10% of expected ν_μ signal events. Hence, a reasonably good moun/pion discrimination is needed in order to perform this measurement.

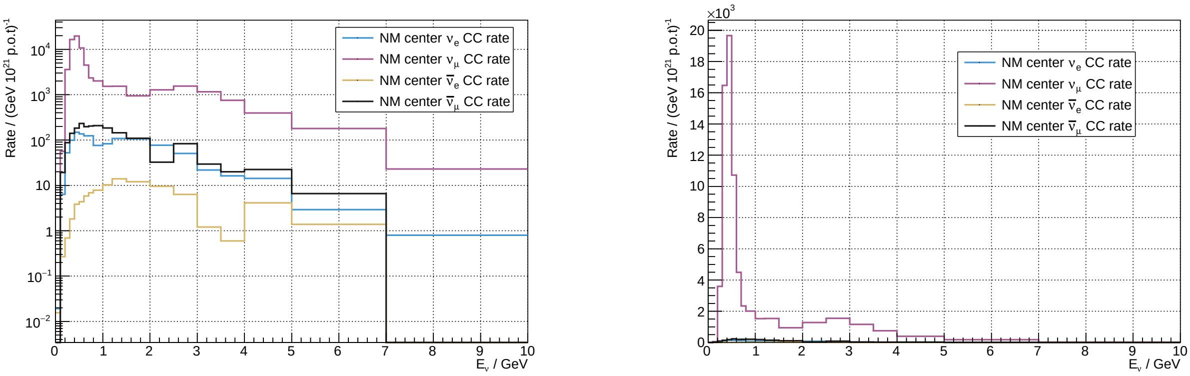

((a)) Logarithmic scale

((b)) Linear scale

Figure 28: Expected CC interaction rate for all flavor components of the J-PARC beam in the neutrino mode at the ground level of the NM building.

Table 4: Expected number of interactions for the NM ground flux for 10^{21} p.o.t. and 500 kg target mass.

Type	Interactions
ν_e CC	291
ν_μ CC	10566
$\overline{\nu}_e$ CC	32
$\overline{\nu}_\mu$ CC	400
ν NC	4833
$\overline{\nu}$ NC	209

A Monte Carlo sample of the ν_μ CC interactions with water induced by the NM ground level flux has been produced using GENIE v3.4.2 and tune G18_02a_00_000. The sample consists of 10^7 interactions. All plots produced using this sample will be normalized to the expected number of events shown in Table 4. For the purposes of this analysis, the interactions have been divided into the low-energy region of interest $E_\nu \leq 0.8$ GeV (shown blue in the plots) and high energy tail $E_\nu > 0.8$ GeV (shown red in the plots). This division as a function of true neutrino energy is shown in Fig. 29.

The muon momentum and cosine scattering angle ($\cos\theta_\mu$) distributions are shown in Fig. 30.

Muons coming from the lower energy part of neutrino spectrum will have lower momentum than those of the high energy tail. The angular distribution of muons from the low energy spectrum will be much more isotropic than that from the high energy part, which strongly prefers forward scattering. This is due to the higher boost required to go from center-of-mass (CM) frame to the laboratory frame. It should be noted that this is valid for neutrinos, but not antineutrinos, since in antineutrino case the muon scattering angle is not isotropic even in the CM frame due to chiral nature of the weak force.

The range of muons coming from the low energy part is estimated to be of the order of 1 m or less, depending on the design of the detector. That means that a large fraction of such events will have a muon track contained within the detector. This is expected to help with rejection of cosmic muons, a topic which will need to be studied in detail as the detector will be placed at ground level.

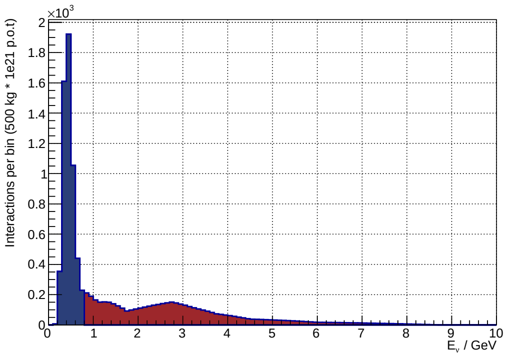

Figure 29: The energy spectrum of simulated ν_μ interactions. Blue region means $E_\nu \leq 0.8\,\mathrm{GeV}$, red one means $E_\nu > 0.8\,\mathrm{GeV}$.

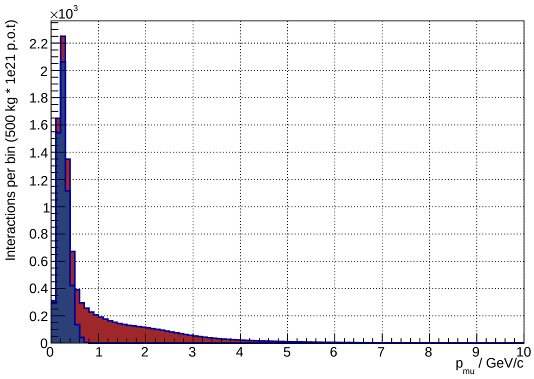

((a)) Muon momentum

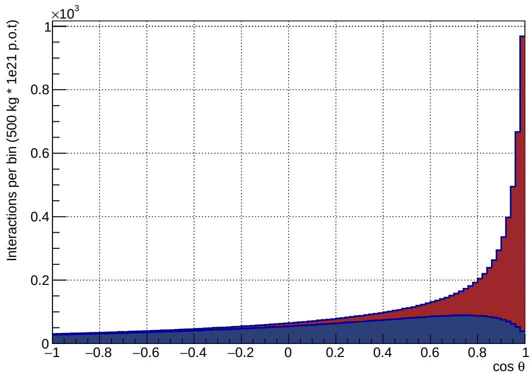

((b)) Cosine of muon scattering angle

Figure 30: Expected distributions of the muon momentum and $\cos\theta_\mu$ from the ν_μ CC interaction at the NM building ground level. Blue distributions come from $E_\nu \leq 0.8\,\mathrm{GeV}$, red ones from $E_\nu > 0.8\,\mathrm{GeV}$. The distributions are plotted stacked on top of each other, such that the total value in each bin represents the number of expected interactions in this bin.

3.3. *Design of the ground level NINJA emulsion detector*

The current design of the water-target NINJA detector is based on alternating plates of: emulsion film, iron, emulsion film, water. The idea for the ground level detector is to replace the iron plate with an emulsion film with thick emulsion layers. The width of a single thick layer of an emulsion could go up to 400 µm, which would be applied on both sides of a plastic base which is itself 60 µm thick. This would make the total width of the thick emulsion film about 0.86 mm. Additionally, if the thick emulsion layer can be doped with halogens using chemically inert compounds that do not affect photographic properties, its density can be increased, thereby enhancing its stopping power. As a result, the momentum reconstruction of charged particles and particle identification (PID) can be improved.

The schematic diagram of the ground level water-target NINJA detector is shown in the Fig. 31.

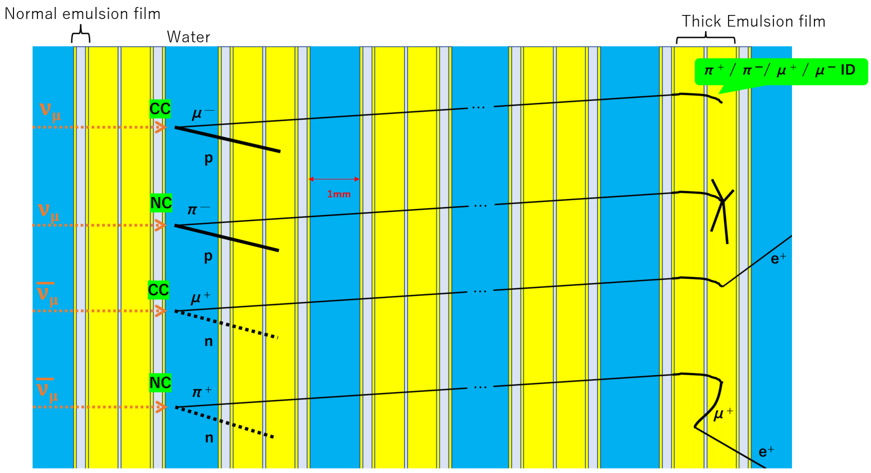

Figure 31: Schematic diagram of the ground level water-target NINJA detector design.

The basic idea for PID in this kind of a detector is to observe the particle stop in the thick emulsion layer. This is why the high density of this layer is desirable. The particle species would be differentiated as follows:

- **negative muon** would be captured by an atom in the emulsion layer. Then it would either decay to a Michel electron or would get captured by the nucleus. In case of nuclear capture the track would abruptly stop, otherwise the Michel electron would be detected. Therefore, if a track abruptly stops in the thick emulsion layer it is a μ^- candidate. The probability for nuclear capture increases with the size of the nucleus, so this is yet another benefit of doping the thick emulsion layer with a high-Z element;
- **positive muon** would stop in the interatomic space in the emulsion layer and then decay at rest to a Michel positron. The signature of this would be a track stopping and producing an electron-like track, which would be tagged as μ^+ candidate;
- **negative pion** would interact with a nucleus in the emulsion layer and produce a *star* made up of hadronic fragments. Hence, a track stopping and producing a *star* is a π^- candidate;
- **positive pion** would stop in the interatomic space in the emulsion and decay at rest to a low-momentum (30 MeV/c) positive muon. This muon would in turn decay at rest after leaving the track of about 600 µm long into a Michel positron, probably within the same emulsion layer. Hence, a track that stops, produces another short low-energy track, which in turn produces a positron-like track is tagged as a π^+ candidate;
- **proton** will leave a highly ionizing and relatively short track which is easy to identify.

This particle identification scheme will make it possible to tag ν_μ CC interactions, in particular to differentiate them from pion-producing NC processes. It should be noted that it could prove difficult to reconstruct the full Michel electron track due to its highly non-linear nature, but it could be feasible to tag it as the low-energy electron/positron track by observing at least a part of it near the muon track stop; this requires further study.

All the discussion in this section assumed a run in neutrino mode of the T2K beam. The antineutrino mode will also be studied, as it provides opportunities to measure phenomena unique to a few 100 MeV antineutrinos like Λ particle production in the energy region where Δ resonance is forbidden (see Sec. 1). In the current planning of future T2K runs, it is foreseen that there will be frequent switching between neutrino and antineutrino mode (in the order of one month each), which will pose a certain challenge to the proposed measurement since the detector will not have any timing capabilities. We have already started devising ideas on how to overcome this challenge, like using different orientations of the detector for neutrino and antineutrino mode or devising a good enough discrimination algorithm between neutrino and antineutrino interactions. This will be studied in detail in the future.

3.4. Summary

Measuring the neutrino interaction cross-sections at the ground level of the NM building at J-PARC would benefit not only the ESSνSB project, but a wider neutrino community as it would for the first time probe the unexplored neutrino energy region of few 100 MeV. The NINJA detector based on thick emulsion is a novel technique which we expect will be able to perform the proposed measurements without relying on external detectors.

4. Heavy-water target run for neutrino-nucleon interaction study

4.1. Introduction

Current and next generation accelerator-based neutrino experiments are poised to answer fundamental questions about neutrinos. Precise neutrino scattering cross sections on target nuclei are critical to the success of these experiments. These cross sections are computed using nucleon-level amplitudes combined with nuclear models. Nuclear models describe the FSIs, interactions inside the neutrino interaction target nucleus. Regardless of whether nuclear corrections are constrained experimentally or derived from first principles, independent knowledge of the elementary nucleon-level amplitudes is essential [84]. The opportunities and the challenges of a new elementary target experiment will be presented.

4.2. Neutrino cross section with a nucleon

Neutrino interaction with a nucleon is an important data with minimum bias from the FSI effects in the target nucleus. While there are difficulties to handle nucleon targets in real experiment. Proton, i.e. Hydrogen can be a liquid or a gas target but dangerous. Neutron is not stable and not suit for a large scale neutrino fixed target. So one need study neutrino-nucleon cross section with molecules having hydrogen isotopes. In that case, neutrino-nucleon interactions data are obtained by subtracting interactions with molecule-B from interactions with molecule-A, where molecule-A have some additional hydrogen isotopes than molecular-B. For example, a plastic (CH) plate as molecule-B and a carbon bulk plate as molecule-A and the study of neutrino-proton interaction can be done by the subtraction A - B method.

Here we are proposing material-A as heavy water and B as light water to study neutrino-neutron interactions, where a neutron is suitable to make ν_μCC interactions. It is important to recall that neutrino CCQE scattering, the primary interaction of many oscillation experiments, can only proceed with a neutron in the initial state: a direct study of this key process needs a neutron target. The neutrino-neutron interactions is a fundamental input to models of neutrino-nucleus interactions in Monte Carlo neutrino event generators.

A deuterium target provides a source of neutrons in a relatively simple and loosely-bound nucleus (binding energy per nucleon is 1.1 MeV, Fig. 32). A deuteron is one of the minimum size nucleus next to a proton and expected to be nearly free from FSIs.

To extract the neutrino interaction with a nucleon data, not only just subtracting number of events with material-B from one of material-A, but also kinematical information to identify the target nucleus can be used. One of such event feature of interactions with heavy nucleus case is multiple protons evaporating form the interacted nucleus by high rate and such evaporated protons will be detected / analyzed by Emulsion Cloud Chamber (ECC hereafter). While CCQE interaction with deuteron case a single proton is expected to be emitted from the interaction. The other nice feature can be used for deuteron CCQE event selection is use of the difference of nucleon Fermi momentum of deuteron and oxygen nucleus. Fermi momentum of deuteron is expected to be significantly small as about 30% of it of oxygen nucleus [85][86]. This Fermi momentum difference can be measured by a geometrical parameter, azimuthal angle

(ϕ) difference between a proton and a muon. A set of deuteron CCQE event selection cuts are understudy by killing oxygen interactions who has larger ϕ difference between a proton and a muon. About a factor of two enhancement of signal event ,deuteron CCQE, is expected.

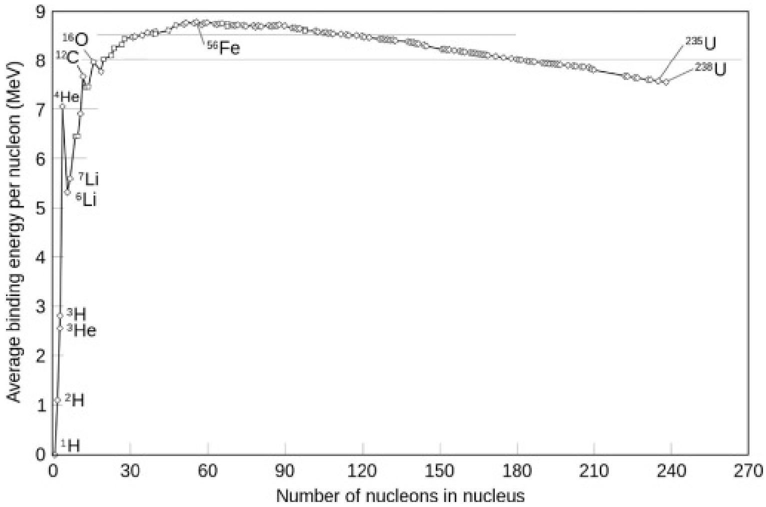

Figure 32: Nuclear Binding Energy. deuterium ^{2} H is the most lowest binding energy nucleus other than proton.

4.2.1. pion production

Recent results from the NINJA iron target run (T60, Run6) [7] have revealed an unexpected excess of backward-going pions, as shown in Fig. 1, highlighting the complexity and richness of hadron measurements in neutrino interactions. Measurements of neutrino interactions on nuclear targets are inherently complicated by the interplay of nuclear and neutrino physics, making it challenging to disentangle issues arising from neutrino interaction cross-section calculations and the modeling of FSIs due to nuclear effects. In contrast, neutrino interaction studies using heavy-water targets offer a clearer view of neutrino-nucleon interactions, providing a valuable baseline for interpreting pion production processes and improving our understanding of these events.

Data on neutrino-deuteron interactions provide fundamental information on neutrino interaction with proton and neutron. It is important as an input for the analysis of the neutrino-nucleus interaction and it also contributes to reveal the nucleon structure and response on the axial current. The 'nuclear effects' of neutrino-deuteron interactions can be rather reliably handled theoretically for the 0π and 1π final states [87] [88] [89]. Even the data in a restricted kinematical region give us an important information.

The data on $\nu_\mu + d \rightarrow \mu^- + p + p$, hereafter d is a deuteron, interactions in the 'QE' kinematical region gives neutrino-neutron interaction in particular axial vector current and its Q^2 dependence. The off the 'QE' region data contribute to clarify the role of meson exchange current(MEC). MEC and '2p2h' is considered as mechanisms to explain the strength between QE and Δ of neutrino-nucleus inclusive cross section. MEC has never verified for the neutrino interaction in GeV region.

For 1π interaction, the strongest interaction $\nu + p \rightarrow \mu^- + \pi^+ + p$ is isospin 3/2 ($I = 3/2$) and is dominated by the excitation of Δ_{1232}. Axial vector strength and it Q^2 evolution of $N\Delta$ transition is important information to be extracted from data. neutrino-proton and neutrino-neutron interactions of neutrino-deuteron interaction lead to the same $\pi^+ pn$ hadronic states. The data of 'QE' region of each interactions lead pion production on both $I = 3/2$ and $I = 1/2$ interaction. Currently, little information is available for the pion production for $I = 1/2$ above Δ_{1232}. They are important information for the analysis of the GeV neutrino-nucleus interaction. An 'elastic' neutrino induced pion production interaction $\nu d \rightarrow \pi^+ d$ (CCπ^+) is interesting which is sensitive to particular, spin-isospin non-flip, part of the axial vector pion production amplitude.

The SS floor, located in the NM building and 280 meters from the neutrino production point at J-PARC, is particularly well-suited for studying pion production interactions. This is due to its ability to generate a neutrino beam with a peak energy of 1 GeV, an energy range that is ideal for probing these interactions.

4.3. *Detector and data analysis*

4.3.1. *A pilot technical run (J-PARC T81): Establishment of the heavy-water treatment*

A pilot analysis of heavy-water interactions with an ECC were carried out by J-PARC T81 (NINJA RUN9). The heavy-water ECCs consist of tracking units and 2.3 mm-thick water target layers as shown in Fig. 33. Each tracking unit consists of two emulsion films on both sides of a 500 μm-thick iron plate. The tracking units and target water layers are placed perpendicularly to the neutrino beam direction. There are 58 heavy-water layers and 70 iron plates in total in the detector. The ECC is an effective detector for the precise measurement of charged particles, with low momentum thresholds of 200 MeV/c and 50 MeV/c for protons and charged pions, thanks to its thin-layered structure. Through the pilot run, we established the treatment of heavy water. Deuterium in heavy water will be easily exchanged ($D_2O + H_2O \rightarrow 2HDO$) by hydrogen atoms from light water in the air atmosphere. An ECC of the same structure with the water ECC of J-PARC E71a but replacing water with 9 kg of heavy water was made under the condition of nitrogen air flow in a glove box. Fig. 34.

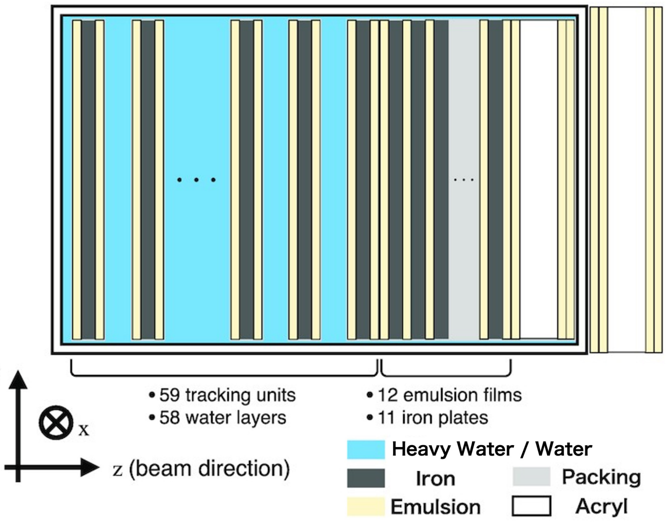

Figure 33: Structure of a heavy-water ECC in the NINJA experiment. Tracking units and 2.3 mm-thick (heavy-) water layers are alternately set perpendicularly to the neutrino beam direction. Each tracking unit consists of two emulsion films on both sides of a 500 μm-thick iron plate.

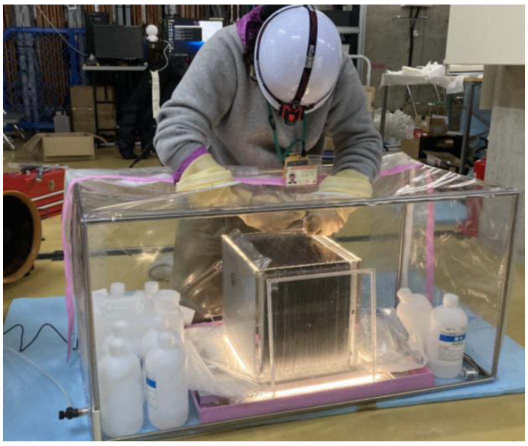

Figure 34: Preparation of heavy-water ECC in a glove box nitrogen atmosphere

The heavy-water ECC was exposed to neutrino beam at the B2 floor from March 2021 and April 2021. A total of 1.78$\times$ 10^{20} POT beam are exposed to the ECC followed with an emulsion time stamper and a scintillation tracker, BabyMind muon spectrometer. After neutrino exposure, the heavy-water target was collected and sent to company for heavy water purity measurement. The purity was about 99.0% and it shows the contamination of hydrogen instead of deuterium is low enough for the aimed experiment. The analysis of the ECC is on going and several neutrino event candidates in heavy water are detected. While it is a pilot technical run to establish the treatment of the heavy-water ECC, so the interacted statistics is too poor to perform extraction of the neutrino-neutron cross section value.

4.3.2. Proposing a heavy-water target experiment

As mentioned in 4.2, a set of event selection to enhance heavy water interactions is understudy. And about a factor two of event concentration is expected. Here experimental setup is designed even if the event selection dose not work for conservatory.

The core idea to measure the neutrino-nucleon cross section is subtraction of the light water interactions from the heavy-water interactions. It is one of statistical analysis and needs relatively large statistic on number of interactions to know the neutrino-nucleon cross section in some accuracy. Fig.35 shows the schematic view of ν_μCC interactions with light and heavy waters. The difference is cased by a neutron in the deuterons.

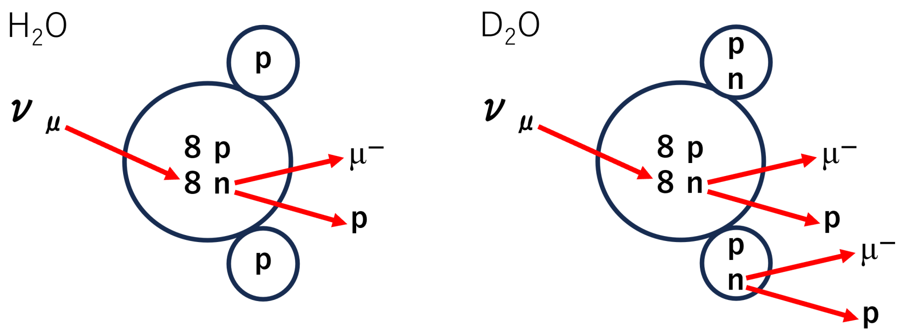

Figure 35: Schematic view of ν_μCC interactions on the light-water and the heavy-water targets. The difference is just a neutron in the deuteron.

We are aiming to measure neutrino-nucleon CC cross section with $\pm$ 5% statistical accuracy. This requirement can be translated to the number of CC interactions in light water and heavy water about 34,900 and 40,300 events respectively and subtracting them 5,400 $\pm$ 270 signal events is considered.

The detectors will be mounted on the SS floor in order to get higher neutrino flux. The $3 \times 3 \times 2$ walls of the ECCs will be mounted in front of an interactive neutrino grid (INGRID)[90, 91], see Fig.36. INGRID is the on-axis near detector for the T2K experiment. INGRID module comprises 11 scintillator planes interleaved with 9 iron plates. The corresponding 300 kg of light- and 334 kg of heavy-water targets. The detector structure of the heavy-water ECC and the water ECC is identical, differing only in whether heavy water or light water is used for the water layers. A total of 72 ECCs using such 4 hybrid with INGRID detector will be irradiated to neutrino beam ($2.8{\times}10^{21}$ POT) in 2 years. The 36 light-water ECCs and the 36 heavy-water ECCs will be mounted in opposite arm to cancel out neutrino energy distribution dependence on each position of the INGRID modules. The total target mass consists of 300 kg of light-water and 334 kg of heavy-water. The SS floor provides a higher neutrino peak energy and a greater neutrino flux compared to the B2 floor, enabling the detection of a larger number of neutrino interactions. Since statistical precision is critical for the subtraction analyses, conducting the heavy-water target experiment on the SS floor is more advantageous.

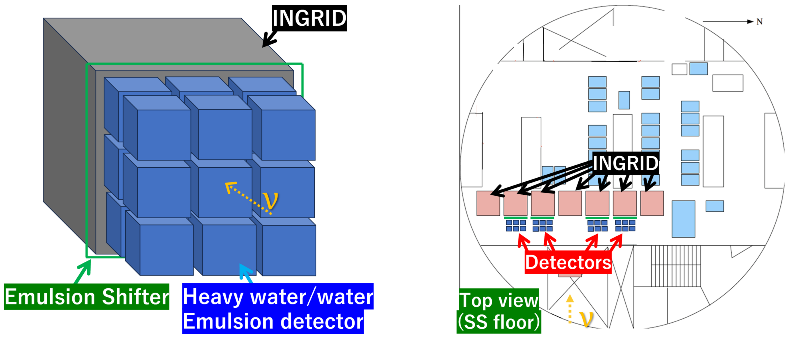

Figure 36: Schematic view of proposed heavy-water run at the SS floor.

Heavy-water ECCs are followed interface tracker to connect muon tracks to the INGRID and the muons from ν_μ CC will be identified with the INGRID. The heavy-water ECCs are just copies of that of pilot run and the treatment of heavy water was already established, while we need treat 72 ECCs, which is about 8 times of E71a, in suitable time. The analysis of neutrino CC location is same with that of pilot run or E71a. After detection of ν_μ CC events in each heavy-water ECCs (n_{HW}) and light-water ECCs (n_{LW}). The number of detected neutrino CC events can be expressed that of par heavy- or light-water molecular number in N_A for easy calculation and N_{HW} and N_{LW}. Approximately N_{HW} - N_{LW} would be the number of neutrino-neutron CC events. The number should be corrected by efficiency for each ECCs, while the efficiencies are expected to be similar or identical. If an event selections was applied case , correction by an additional section efficiencies will be applied.

Subtracting a kinematical parameter distribution of light water from heavy water will show the distribution of neutrino-neutrino interaction. A detailed analysis on neutrino-neutron will be done with such a subtraction of histograms.

The majority of neutrino interactions are CCQE interactions. In that case no multiple production of pions are associated to the events. Naively just a proton and muon are produced at the CCQE interaction. The behavior of produced protons are expected to be different in the neutrino-oxygen CCQE and neutrino-neutron CCQE, since large effect from FSIs in an oxygen nucleus case but almost free with a neutron interactions. These differences will be analyzed by subtraction of histograms on proton angle distribution.

In non quasi-elastic CC cases, pions are associated to the neutrino interactions. The same story is valid for produced pions in the neutrino-oxygen and the neutrino-neutron CC interactions. A proton and a pion angle distribution made by subtracted histograms will be analyzed.

Since the amount of ECCs is about 8 times of E71a, the speed up of the analysis is required from the scanning films to event analysis. Concerning about speed up of scanning, development with a new scanning system HTS2 is on going. The expected scanning speed in near future will be about 5 times of current system HTS1. Together with the track data readout from films, speedup of processing is on-going to follow with the scanning speed. So the analysis of this proposed experiment is expected to be handled in reasonable time scale of a few years.

4.4. Discussion

In the heavy-water target run, nuclear effects can be studied through measurements of neutrino-induced hadrons. This heavy-water target run utilizes both heavy-water ECCs and water ECCs. These ECCs incorporate iron plates, which serve as structural supports for the emulsion films and are also used for momentum measurements. Notably, these iron plates can be utilized as a target material to study nuclear effects. Nuclear effects, which are expected to increase with the mass of the target nucleus, can be indirectly measured by comparing neutrino interactions on different target nuclei. Fig. 37 presents the momentum distributions of protons from CC$0\pi1p$ events induced by ν_μ interactions with water and iron targets, while Fig. 38 shows the differences between these momentum distributions. In neutrino interactions, protons are expected to experience a momentum shift from higher to lower momentum due to FSIs as they propagate through the nucleus. In the high-momentum region ($400\,\mathrm{MeV}/c - 600\,\mathrm{MeV}/c$), the number of protons from neutrino-iron interactions is observed to be smaller than that from neutrino-water interactions. Conversely, in the low-momentum region ($200\,\mathrm{MeV}/c - 400\,\mathrm{MeV}/c$), the number of protons from neutrino-iron interactions exceeds that from neutrino-water interactions. This behavior is attributed to the stronger momentum shift caused by FSIs in the iron target compared to the water target, reflecting the greater nuclear effect in the former. Thus, neutrino-induced protons serve as a valuable probe for studying FSIs and nuclear effects. The ECC detector, in particular, has the capability to measure low-momentum protons down to $200\,\mathrm{MeV}/c$, which are critical for gaining insights into FSIs and advancing our understanding of nuclear effects.

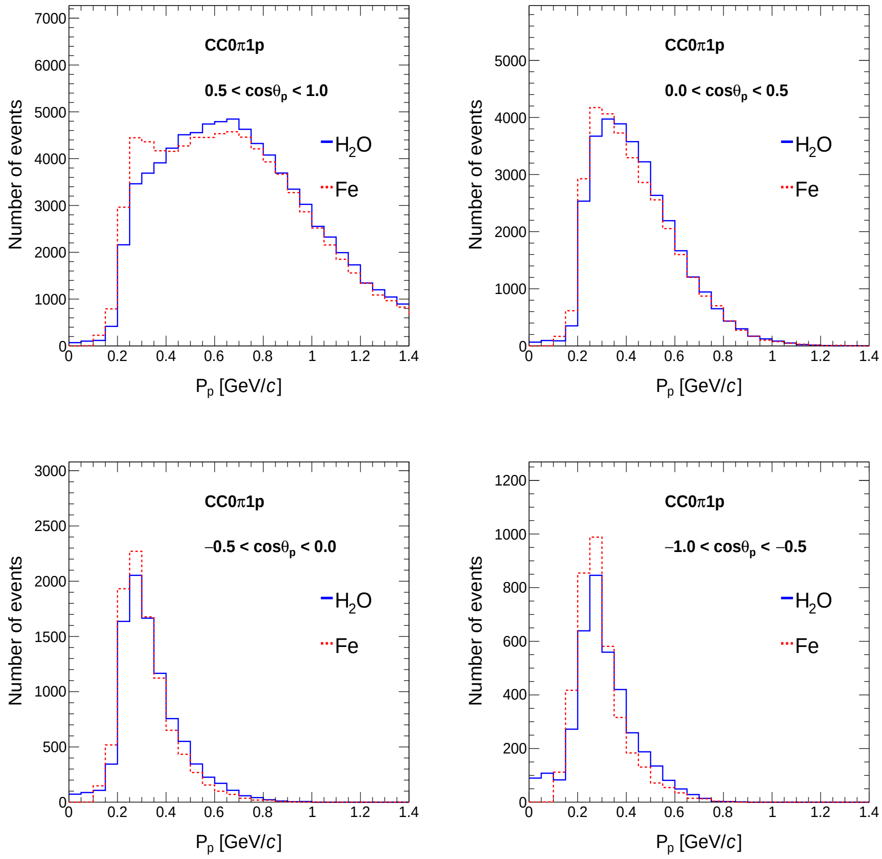

Figure 37: Momentum distributions of protons in CC0π1p events induced from neutrino-water and neutrino-iron interactions. The angular region is divided into four segments. Each plot shows the momentum distribution of protons within the specified angular range. The numbers of events are normalized to the expected number of neutrino interactions in a water target, assuming a neutrino beam exposure of 1.0×10^{21} POT in the heavy-water target run.

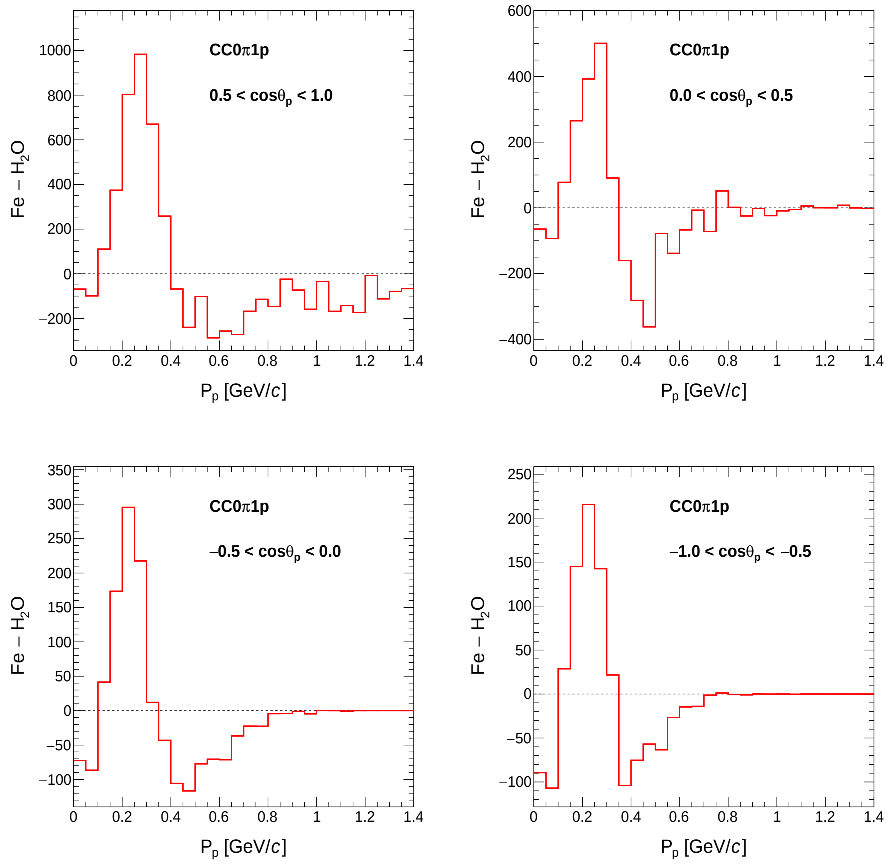

Figure 38: Difference of proton momentum distributions between neutrino-water and neutrino-iron interactions. The event samples are CC0π1p events. The angular region is divided into four segments. Each plot shows the difference of the proton momentum distributions within the specified angular range. The vertical axis is the difference between the number of expected events for neutrino-iron interactions and that for neutrino-water interactions. The number of neutrino-iron interactions is normalized to that of neutrino-water interactions, assuming a neutrino beam exposure of 1.0×10^{21} POT in the heavy-water target run.

The heavy-water ECCs enable the study of pure 2p2h interactions. Fig. 39 shows an opening angle between two protons of ν_μ-iron CC0π2p events in the NINJA iron-target run (T60, Run6). The two protons generated by the 2p2h interactions are expected to exhibit back-to-back emissions [92]. However, there were fewer back-to-back protons in the data than in the MC prediction, while there were more protons in the same direction in the data than in the MC prediction, although the statistical uncertainty was large. It can be considered that the back-to-back protons may be induced incidentally by FSIs rather than the physical processes of the 2p2h interactions. While nuclear effects are expected to have a significant impact on neutrino-iron interactions, their influence on neutrino-deuteron interactions is anticipated to be minimal. A neutron inside a deuteron is treated as nearly free nucleon above. While a proton and a neutron in the deuteron are bonded. An CC 2p2h like event, a muon and two protons, can be considered and studied in neutrino-deuteron interaction. We can expect pure 2p2h events by deuteron nucleus target since a deuteron nucleus is the smallest one which can create a 2p2h event. Using a muon and two protons events, two protons correlation on angle, momentum can be studied.

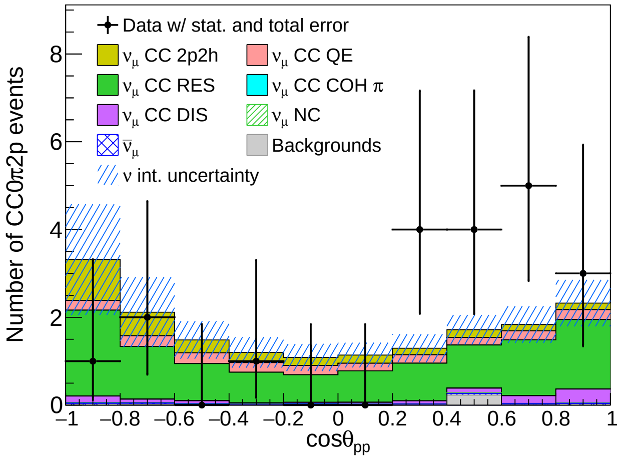

Figure 39: Opening angle between two protons in ν_μ-iron CC0π2p events measured by the NINJA iron-target run (T60, Run6)[3]. Back-to-back protons are in $\cos\theta = -1$, whereas protons emitted in the same direction are in $\cos\theta = 1$.

4.5. Summary

We propose a neutrino-nucleon interaction measurement using the heavy-water ECCs at the SS floor in the J-PARC's NM building. Neutrino interaction with a nucleon is an important data with minimum bias from the FSI effects of the target nucleus. Neutron in a deuteron is quasi-free nucleon as well as quasi-free from FSIs, and the neutrino-neutron interactions can be measured using the heavy-water ECCs. The key to measuring the neutrino-nucleon cross section lies in the statistical subtraction of results from light-water interactions from those of heavy-water interactions. In the heavy-water target run, with a total target mass of 300,kg of light-water and 334,kg of heavy-water, and an exposure of $2.8{\times}10^{21}$ POT over two years, the number of statistically subtracted events corresponding to neutrino-neutron interactions is about $5,000 \pm 270$. Specific event feature differences between heavy nucleus and deuteron, number of evaporating protons from target nucleus proton azimuthal angle respect to muon azimuthal angle angle etc, are under study and will be used for signal event enhancement.

Although the treating amount of the ECCs is about 8 times of E71a, the scanning speed will be improved by new scanning system HTS2 and improvement of processing data speed and the events analysis speed can be managed. The distribution of angle and momentum of partner hadrons, protons and pions, will be used to enhance the signal events and could be analyzed in detail to know the neutrino-nucleon interaction or FSIs with comparing that of light-water interaction sample. A deuteron binding effect could be also tested through two protons emission events like 2p2h candidates. In addition, comparing the results of neutrino interactions in the light-water ECCs with those in the iron target layers will help elucidate the effects of FSIs on neutrino-nucleon interactions. The NINJA heavy-water target run is expected to offer a clearer understanding of neutrino-nucleon interactions and provide critical insights into modern neutrino interaction models.

5. Sterile neutrino search

5.1. Physics background

The possibility of having more than three neutrinos in nature has been discussed for a long time among the physics community. If there exists a fourth neutrino, then it has to be sterile and could mix with three active neutrinos. Several experimental anomalies hint towards an extra sterile neutrino [93]. Key anomalies, being the backbone of sterile neutrinos, are LSND anomaly [94], where a significant excess of events has been observed beyond known backgrounds, MiniBooNE [95] low-energy excess seen during charged pion decay in flight. Reactor [96] and Gallium [97] anomalies, related to an overall normalization discrepancy in electron antineutrinos, also point towards the sterile neutrino hypothesis. Recent results of MicroBooNE [98] experiment found no evidence for the light sterile neutrino.

However, a combined analysis of MiniBooNE and MicroBooNE data shows that the 3+1 model is still allowed at a significant confidence level [99]. Beyond accelerator results, gallium-based experiment BEST [100] and reactor-based experiment Neutrino-4 [101] recently reported a positive signal for a light sterile neutrino. On the other hand, data from IceCube [102], Daya Bay-MINOS [103], T2K [104], NOνA [105], STEREO-PROSPECT-DANSS [106], NEOS [107] and DeepCore [108] is consistent with the no sterile neutrino hypothesis. Several upcoming experiments, such as JSNS^2 [109], ICARUS [110] and SBND within the Fermilab short-baseline program, are dedicated to the search for sterile neutrinos. From this discussions, it is clear that the existence of the light sterile neutrino remains intriguing question, and in need of the further investigation in all possible directions.

In this proposal, we outline the potential to search for sterile neutrinos in the NINJA experiment. Though the primary goal of NINJA is to measure cross-section, the distance of the NINJA detector from the neutrino source at J-PARC provides an ideal opportunity to search for eV scale sterile neutrinos at NINJA experiment. In the next section we provide the theoretical framework for the sterile neutrino hypothesis and then we outline the experimental configuration of NINJA which we consider in our analysis. After that we present our results and then we summarize our findings.

5.2. Framework

In presence of a light sterile neutrino, the unitary PMNS matrix U which relates the neutrino flavour states to the mass states, is written in the following way:

$$U = U_{34}(\theta_{34}, \delta_{34}) U_{24}(\theta_{24}, \delta_{24}) U_{14}(\theta_{14}, 0) U^{3\nu}\,, \tag{9}$$

$$\text{with} \quad U^{3\nu} = U_{23}(\theta_{23}, 0) U_{13}(\theta_{13}, \delta_{\rm CP}) U_{12}(\theta_{12}, 0)\,, \tag{10}$$

where $U_{ij}(\theta_{ij}, \delta_{ij})$ denotes a rotation in the (i, j)-plane with mixing angle θ_{ij} and phase δ_{ij}. Neutrino oscillation in the standard three flavour is governed by three mixing angles: θ_{13}, θ_{12} and θ_{23}, two mass squared differences: $\Delta m^2_{21} = m^2_2 - m^2_1$ and $\Delta m^2_{31} = m^2_3 - m^2_1$ and one phase: $\delta_{\rm CP}$. In the presence of a sterile neutrino, this mixing scheme is extended by three new mixing angles: θ_{14}, θ_{24} and θ_{34}, two additional phases: δ_{24} and δ_{34} and one more mass squared difference: Δm^2_{41}.

The appearance channel probability formula in presence of sterile neutrino relevant for NINJA can be expressed as [111].

$$P_{\mu e} = \sin^2 2\theta_{\mu e} \sin^2\left(\frac{\Delta m^2_{41} L}{4E_\nu}\right) \tag{11}$$

with $\sin^2 2\theta_{\mu e} = \sin^2 2\theta_{14} \sin^2\theta_{24}$. Here E_ν is neutrino energy and L is the baseline length. In this proposal, we will show our preliminary results on the capability of NINJA to constrain these parameters $\sin^2 2\theta_{\mu e}$ and Δm^2_{41}.

5.3. Simulation Details

For our estimation, we considered three detector locations: (i) B2 floor (1.5° off-axis), (ii) SS floor (on-axis), and (iii) GROUND floor (6° off-axis) in the NM building, assuming 280 m distance from the neutrino production point at J-PARC. Our flux corresponds to 10^{21} POT per year. For detector response, we used the detector efficiencies from the ESSνSB experiment [77] and we listed them in Tab 5. For the detector target we assumed lead target. We have considered different exposures in the units of "ton-year" to optimize our sensitivity. In our calculations, we have considered Gaussian energy resolution with a width of 10%. For systematic uncertainty, we included an overall normalization error of 5% for the signal and 10% for the background. In our analysis, we have included both appearance and disappearance channel. However, the main sensitivity in the $\sin^2 2\theta_{\mu e}$ - Δm^2_{41} plane comes from the appearance channel.

5.4. Results

In Fig. 40, we have shown the appearance channel probability for sterile neutrinos as a function of neutrino energy for different mass square differences (dashed curves). The fluxes for the three positions of the detectors are shown by solid curves. The value of θ_{14} and θ_{24} is assumed to be 5° in the figure. From this figure, we notice that if the

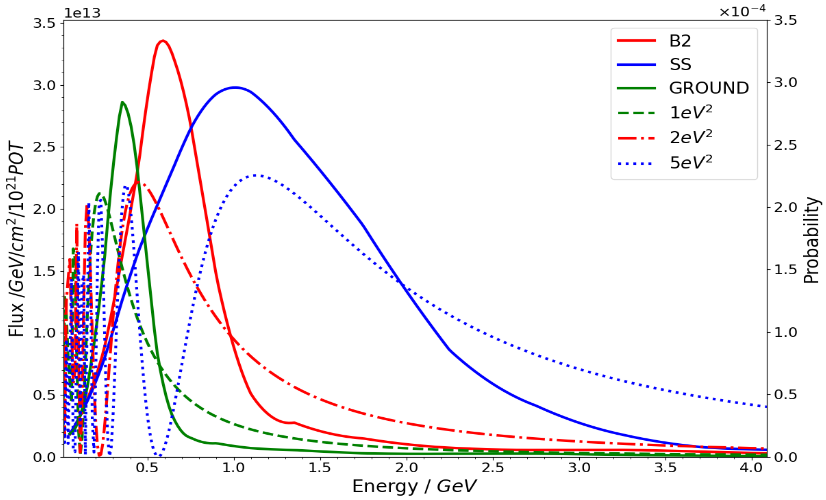

Figure 40: Probability (right y-axis), presented with dashed lines, and flux (left y-axis), presented with solid lines, relevant for NINJA.

detector is located at the B2 floor then NINJA will be sensitive to the mass square difference of 2 eV^2 as in this case the probability peak and the flux peak occurs around the same energy region. Similarly, for the SS floor, NINJA will be sensitive to 5 eV^2 and for Ground floor, it will be sensitive to 1 eV^2.

In Fig. 41, we have shown the expected sensitivity of NINJA to constrain the sterile mixing parameters in the $\sin^2 2\theta_{\mu e}$ - Δm^2_{41} plane assuming a lead target. In the left panel, we considered three detector locations with an exposure of 10 ton-year. From this panel, we see that as expected from Fig. 40, ground floor is sensitive to approximately 1 eV^2, the B2 floor is sensitive to 2 eV^2 and SS floor is sensitive to 5 eV^2. An interesting point is that with the SS floor option, NINJA will be able to place stronger constraints on the sterile mixing parameters compared to the current limits from MicroBooNE [112], while the bound from the ground floor is weaker and the B2 bound is comparable to the current one. The reason for this behavior becomes clear by examining Tab. 5, where we present the number of signal and background events for all the three locations of the NINJA detector. This table shows that the number of signal events for the SS floor are higher than the number of events of the B2 floor and Ground floor. It also reveals that most of the background in all cases comes from the intrinsic electron neutrino beam, followed by misidentified muons (mis-id) and neutral current (NC) events. Since the SS floor provides the best sensitivity for sterile neutrinos, in the right panel of Fig. 41 we show the sensitivity at the SS floor considering different exposures. From this panel, we show that even with 4 ton-year exposure, it is possible to obtain a stronger bound than MicroBooNE for Δm^2_{41} around 5 eV^2 with the SS floor.

To understand the role of the background for the SS floor, in the left panel of Fig. 42, we show the spectra for both signal and background events. This panel is generated for Δm^2_{41} = 5 eV^2 and $\sin^2 2\theta_{\mu e}$ = 0.001. From this panel, we observe that above 2 GeV, signal events become much less frequent, whereas the number of background events remains quite significant. Therefore, if we apply an upper energy cut around 2 GeV, we may obtain better sensitivity due to a higher signal-to-background ratio. To illustrate this, in the right panel, we show the sensitivity for various energy cuts. The blue curve corresponds to the case with no energy cut (10 GeV), while the red and green curves correspond to the cases when energy cuts are applied at 2 GeV and 3.5 GeV, respectively. From the panel, we see that when we apply energy cuts, the sensitivity deteriorates compared to the case with no energy cut. This suggests that even at energies beyond 3.5 GeV, the small number of signal events plays a crucial role in the sensitivity.

Next we study the effect of efficiencies. In generating Figs.41 and 42, we have used the signal and background efficiencies from the ESSνSB experiment. However, for the NINJA experiment, the efficiencies may be different due to slightly different detector technology in NINJA compared to ESSνSB. To study this effect, we considered different sets of efficiencies corresponding to the mis-id and NC backgrounds. Because ESSνSB energies are lower than those

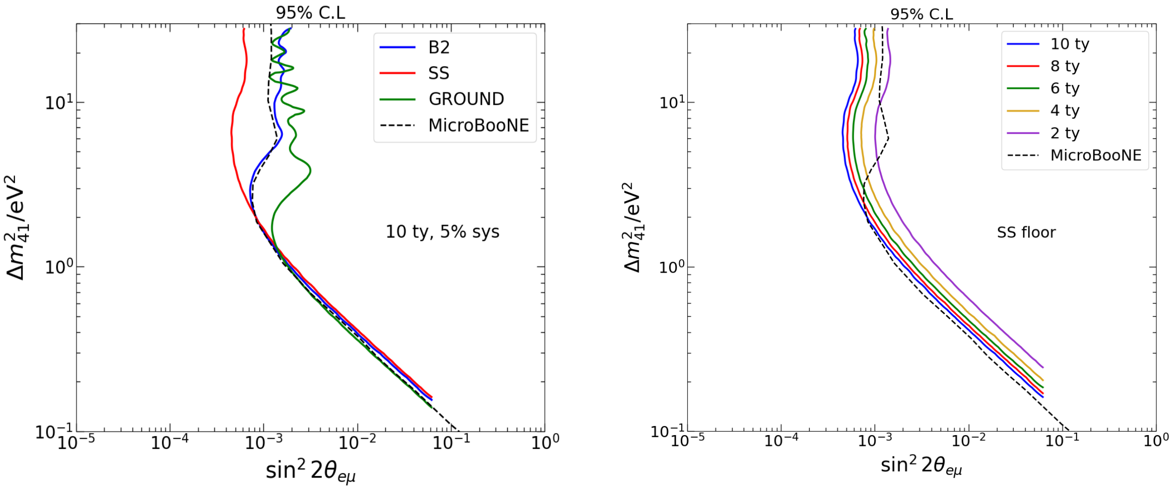

Figure 41: Bounds on the sterile mixing parameters. Left panel: sensitivity for the three locations of the detector using a exposure of 10 ton-year. Right panel: Sensitivity for different exposures for the SS floor.

			APPERANCE CH. (0.95@ $\nu_\mu \to \nu_e$)				DISAPPERANCE CH. (0.95@ $\nu_\mu \to \nu_\mu$)			
			DETECTOR EFFICIENCY (%)	EVENTS (10 ty, L=280 m) B2 $\Delta m^2_{41} = 2eV^2$	SS $\Delta m^2_{41} = 5eV^2$	GR $\Delta m^2_{41} = 1eV^2$	DETECTOR EFFICIENCY (%)	EVENTS (10 ty, L=280 m) B2 $\Delta m^2_{41} = 2eV^2$	SS $\Delta m^2_{41} = 5eV^2$	GR $\Delta m^2_{41} = 1eV^2$
BACKGROUNDS	INTRINSIC BEAM	$\nu_e \to \nu_e$	100	15372.2	29738.3	6089.58	/	/	/	/
	MIS-ID	$\nu_\mu \to \nu_\mu$	1 (0.5)	9342.77 (4471.39)	37369.6 (18684.8)	2190.43 (1095.215)	/	/	/	/
		$\nu_e \to \nu_\mu$	1 (0.5)	0.044 (0.022)	0.166 (0.083)	0.008 (0.004)	/	/	/	/
		$\nu_\mu \to \nu_e$	/	/	/	/	1 (0.5)	5.78 (2.89)	30.09 (15.045)	0.95 (0.475)
		$\nu_e \to \nu_e$	/	/	/	/	1 (0.5)	153.722 (76.861)	297.383 (148.692)	60.9 (30.45)
	NC	$\nu_\mu \to \nu_e$	0.5 (1)	1.006 (2.012)	4.867 (9.734)	0.2 (0.4)	1 (0.5)	1.005 (2.01)	4.87 (9.74)	0.2 (0.4)
		$\nu_\mu \to \nu_\mu$	0.5 (1)	1665.5 (3331)	6253.51 (12507.02)	445.078 (890.156)	1 (0.5)	1665.5 (3331)	6253.51 (12507.02)	445.078 (890.156)
		$\nu_\mu \to \nu_\tau$	0.5 (1)	0	0	0	1 (0.5)	0	0	0
	WRONG SIGN	$\bar\nu_\mu \to \bar\nu_e$	100	5.96	29.36	0.91	/	/	/	/
		$\bar\nu_e \to \bar\nu_e$	100	1171.46	1371.01	508.081	/	/	/	/
		$\bar\nu_\mu \to \bar\nu_\mu$	/	/	/	/	100	21877.8	50151.9	5610.75
		$\bar\nu_e \to \bar\nu_\mu$	/	/	/	/	100	0.125	0.559	0.03
	SIGNAL			549.468	2858.12	90.282		887563	3.55e+06	208091

Table 5: Detector efficiencies and number of expected events for both signal and background. Events are shown for a exposure of 10 ton-year and for all the three flux options. The detector efficiency is taken from the ESSνSB experiment. The number in the parenthesis in the "detector efficiency" column refers to the possible alternate values for NINJA. Events are generated for $\sin^2 2\theta_{\mu e} = 0.001$.

of NINJA (SS), we expect better muon identification in this higher energy region, which will result in a lower mis-id background. On the other hand, in this energy region, it might be difficult to separate the electron signal events and the decay products of π^0, so we expect the efficiency to reject the NC background to be worse than ESSνSB (cf. the numbers in parentheses in the "detector efficiency" column of Tab.5). Our estimation of the sensitivity with these new efficiencies is shown in Fig. 43. From the left panel, we see that the new efficiencies provide slightly better sensitivity compared to the ESSνSB (old) ones. To understand which background, between mis-id and NC, affects the sensitivity

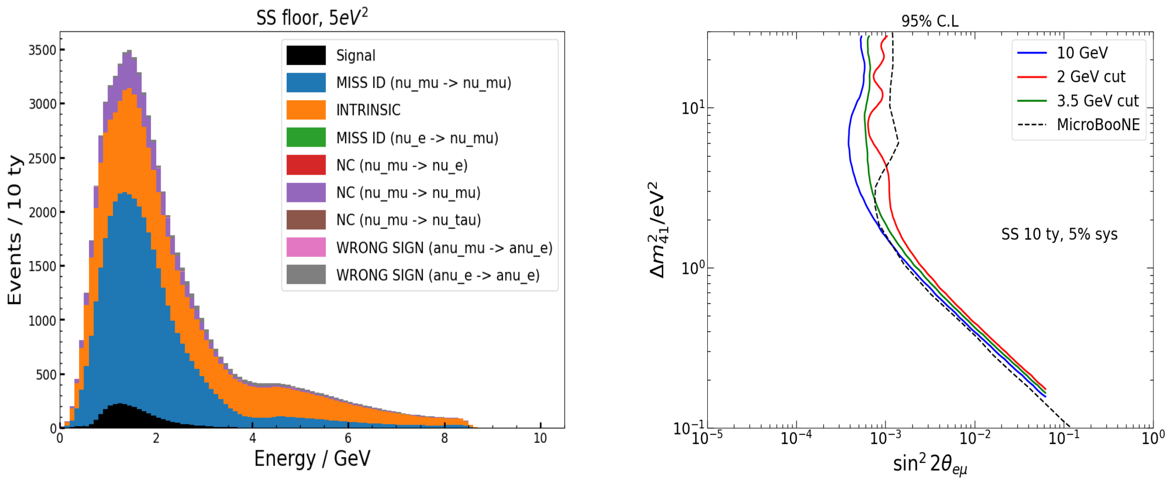

Figure 42: Left panel: Event spectra for signal and background for SS floor Right panel: Sensitivity without (10 GeV) and with energy cuts.

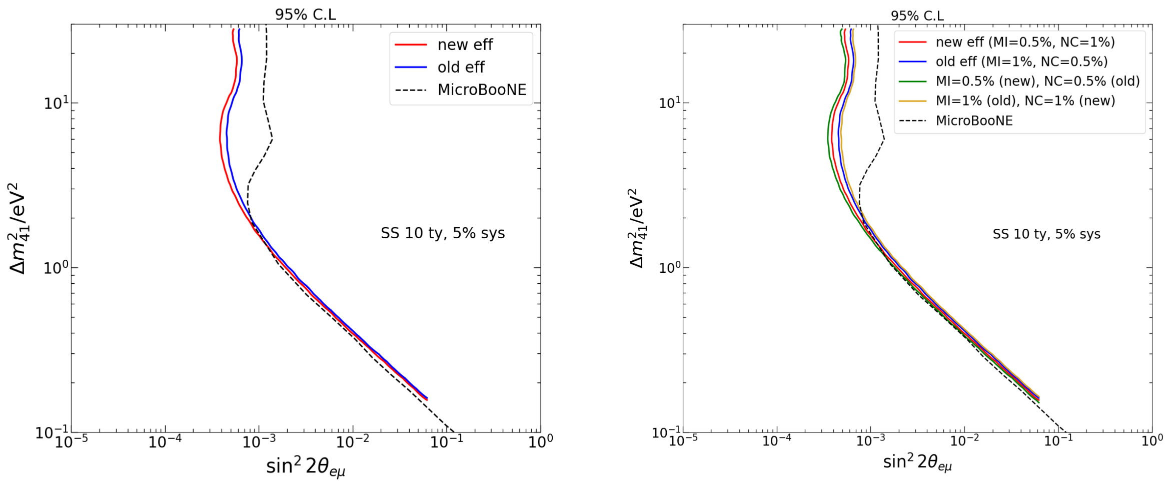

Figure 43: Bounds on the sterile mixing parameters. Left panel: Comparison of old and new efficiencies. Right panel: Comparison one by one.

more, in the right panel we consider one new efficiency at a time. From this panel, we note that the mis-id background affects the sensitivity more than the NC background. We would also like to mention that there are plans to obtain more realistic efficiencies using data from the future RUN 6 iron ECC, which we will incorporate into our future study.

Next, we study the effect of systematics. As there will be no near detector for NINJA, the flux from the J-PARC source will not be measured very accurately. Therefore, in the absence of flux measurement, the systematic error associated with the NINJA experiment can be quite large. To understand this, in the left panel of Fig. 44, we have plotted the sensitivity for four different values of the overall normalization error. From this panel, we see that when the systematics change from 5% to 20%, the change in sensitivity is very small. This signifies that the sensitivity of NINJA is mainly dominated by statistical error. In the right panel of this same figure, we studied the combined sensitivity of NINJA by considering 5 ton-year exposure at the SS floor and 5 ton-year exposure at the B2 floor. This configuration serves two purposes. Firstly, by considering both flux options simultaneously, NINJA will become

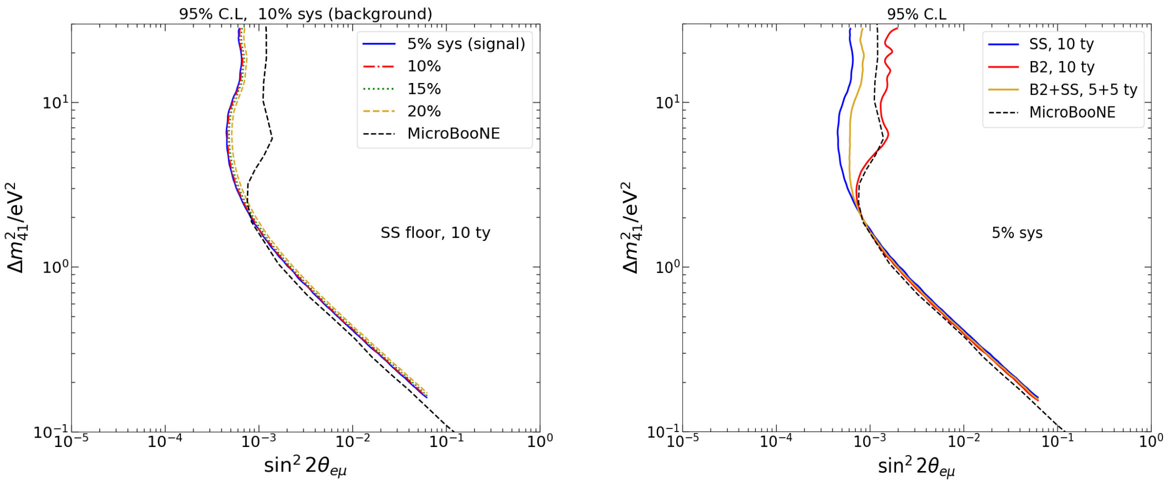

Figure 44: Left panel: Bounds on the sterile mixing parameters for different values of systematic uncertainties. Right panel: Sensitivity when half of the detector is placed in SS floor and half of the detector is placed at B2 floor.

sensitive to a very wide range of Δm^2_{41}. Secondly, in case the SS floor is not sufficient to host a large volume of the NINJA detector, the detector volume can be divided between two locations. From the panel, we see that the sensitivity of the B2+SS floor configuration is sensitive to a wide range of Δm^2_{41} compared to the SS floor-only and B2 floor-only options. However, in this case, the sensitivity is somewhere between the SS floor and B2 floor sensitivities.

5.5. *Summary*

In this LOI, we have shown the potential of NINJA to search for eV-scale sterile neutrinos. Our analysis shows that with a 10 ton-year exposure, the SS floor flux option can provide a better bound on the sterile mixing parameters than the current one, whereas for the B2 (ground) floor, the sensitivity is comparable (or weaker) compared to the current limit. For the SS floor, even with a nominal exposure of 4 ton-year, NINJA will be able to provide a better limit than the current one. Additionally, our analysis shows that (i) placing an upper energy cut does not improve the sensitivity of the SS floor further, (ii) the mis-id background can affect the sensitivity of NINJA, and (iii) the sensitivity of NINJA is dominated by statistical error. Finally, we also show that dividing the exposure equally between the SS and B2 floors can still provide better sensitivity than the current one.

Finally, we would like to point out that if sterile neutrinos exist in nature, the ν_e cross-section measurement from the intrinsic ν_e flux of NINJA will be confused with ν_e events coming from the oscillation of sterile neutrinos in the ν_μ flux. One way to resolve this confusion would be to calculate the cross-section in the energy region where the probability of sterile neutrino oscillation is very small for a given flux option.

6. Conclusions

This Letter of Intent (LOI) detailed the physics goals of the NINJA experiment for the next decade, outlining four specific research projects.

- We propose a neutrino-nucleus interaction experiment using J-PARC's neutrino beamline, directly benefiting T2K and HK experiments. The NINJA detector's proven exceptional tracking of low-energy particles enables unprecedented precision in studying nuclear effects. This capability will allow first-time precision measurements of multi-nucleon knockout in water, investigation of T2K and SK tensions regarding low-energy pion production, and pioneering measurements of nuclear fragment yields to understand de-excitation and final-state interactions. These results will help validate theoretical models and constrain experimental uncertainties, particularly in establishing correlations between neutrino-Carbon and neutrino-Oxygen interactions, critical for improving neutrino oscillation measurements and enhancing their sensitivity.

- A measurement of the neutrino-water interaction cross section measurement is proposed in the lower energy region of about 60-600 MeV. This energy region coincides with the neutrino flux at the near detector site of the proposed future ESSνSB experiment. This would benefit not only ESSνSB, but a wider neutrino community as it would be a first direct experimental probe of the unexplored neutrino energy region of a few 100 MeV. It has been shown that a good position for the detector would be at the ground floor of the NM building, corresponding to the off-axis angle of about 6°. To meet the challenges posed by this low energy measurements, in particular the fact that muon tracks will be contained in the detector, a novel technique of thick emulsion is proposed. We expect that a NINJA detector based on this technique will be able to perform the proposed measurement without relying on external detectors.

- We propose a neutrino-nucleon interaction measurement using the heavy-water ECCs at the SS floor in the J-PARC's NM building. Neutrino interactions with a nucleon provide an important data of minimum bias from the FSI effects of the target nucleus. Neutron in a deuteron is quasi-free nucleon as well as quasi-free from FSIs, and the neutrino-neutron interaction can be measured using the heavy-water ECCs. The key to measuring the neutrino-nucleon cross section lies in the statistical subtraction of results from light-water interactions from those of heavy-water interactions. In the heavy-water target run, with a total target mass of 300,kg of light-water and 334,kg of heavy-water, and an exposure of 2.8×10^{21} POT over two years, the number of statistically subtracted events corresponding to neutrino-neutron interactions is $5,000 \pm 270$. The NINJA heavy-water target run is expected to offer a clearer understanding of neutrino-nucleon interactions and provide critical insights into modern neutrino interaction models.

- We propose an experiment to search for light sterile neutrinos at the eV scale using the NINJA detector and the neutrino source from J-PARC. The distance between the NINJA detector and the neutrino source, along with the energy of the neutrinos from J-PARC, provides an excellent opportunity to search for light sterile neutrinos in this setup. In this proposal, we demonstrate the capability of the NINJA setup to search for sterile neutrinos by considering three different detector locations, varying exposures measured in ton-years. Our results show that NINJA can set more stringent bounds on the sterile neutrino mixing parameters compared to the existing limits, using a realistic and feasible experimental configuration.

Moving forward, we plan to adjust schedules for each project, advance the necessary technological developments, and coordinate/collaborate with J-PARC facilities and related research groups. Additionally, efforts will be made to secure funding, leading to the submission of more concrete research proposals to J-PARC Program Advisory Committee.

References

[1] A. Hiramoto et al. First measurement of $\bar{\nu}_\mu$ and ν_μ charged-current inclusive interactions on water using a nuclear emulsion detector. *Phys. Rev. D*, 102(7):072006, 2020.

[2] H. Oshima et al. First measurement using a nuclear emulsion detector of the ν_μ charged-current cross section on iron around the 1 GeV energy region. *PTEP*, 2021(3):033C01, 2021.

[3] H. Oshima et al. Measurements of protons and charged pions emitted from $\nu\mu$ charged-current interactions on iron at a mean neutrino energy of 1.49 GeV using a nuclear emulsion detector. *Phys. Rev. D*, 106(3):032016, 2022.

[4] K. Abe et al. Constraint on the matter–antimatter symmetry-violating phase in neutrino oscillations. *Nature*, 580(7803):339–344, 2020. [Erratum: Nature 583, E16 (2020)].

[5] K. Abe et al. Hyper-Kamiokande Design Report. 5 2018.

[6] C. A. Argüelles, P. Fernández, I. Martínez-Soler, and M. Jin. Measuring Oscillations with a Million Atmospheric Neutrinos. *Phys. Rev. X*, 13(4):041055, 2023.

[7] H. Oshima et al. Current Status and Results from the NINJA Experiment. The 24th International Workshop on Neutrinos From Accelerators (NuFact 2023), August, 2023.

[8] A. Alekou et al. Updated physics performance of the ESSnuSB experiment: ESSnuSB collaboration. *Eur. Phys. J. C*, 81(12):1130, 2021.

[9] M. G. Aartsen et al. Combined sensitivity to the neutrino mass ordering with JUNO, the IceCube Upgrade, and PINGU. *Phys. Rev. D*, 101(3):032006, 2020.

[10] S. Aiello et al. Determining the neutrino mass ordering and oscillation parameters with KM3NeT/ORCA. *Eur. Phys. J. C*, 82(1):26, 2022.

[11] Aaron S. Meyer, André Walker-Loud, and Callum Wilkinson. Status of Lattice QCD Determination of Nucleon Form Factors and their Relevance for the Few-GeV Neutrino Program. *Ann. Rev. Nucl. Part. Sci.*, 72:205–232, 2022.

[12] S. X. Nakamura, H. Kamano, and T. Sato. Dynamical coupled-channels model for neutrino-induced meson productions in resonance region. *Phys. Rev. D*, 92(7):074024, 2015.

[13] P. Abratenko et al. First Measurement of Quasielastic Λ Baryon Production in Muon Antineutrino Interactions in the MicroBooNE Detector. *Phys. Rev. Lett.*, 130(23):231802, 2023.

[14] A. Fatima, M. Sajjad Athar, and S. K. Singh. $\bar{\nu}_\mu$ induced quasielastic production of hyperons leading to pions. *Eur. Phys. J. ST*, 230(24):4391–4403, 2021.

[15] P. Abratenko et al. Search for long-lived heavy neutral leptons and Higgs portal scalars decaying in the MicroBooNE detector. *Phys. Rev. D*, 106(9):092006, 2022.

[16] A. A. Aguilar-Arevalo et al. Prospects for detecting axionlike particles at the Coherent CAPTAIN-Mills experiment. *Phys. Rev. D*, 107(9):095036, 2023.

[17] T. Fukuda et al. First neutrino event detection with nuclear emulsion at J-PARC neutrino beamline. *PTEP*, 2017(6):063C02, 2017.

[18] Gerald R. Lynch and Orin I. Dahl. Approximations to multiple Coulomb scattering. *Nucl. Instrum. Meth. B*, 58:6–10, 1991.

[19] T. Toshito et al. Charge identification of highly ionizing particles in desensitized nuclear emulsion using high speed read-out system. *Nucl. Instrum. Meth. A*, 556:482–489, 2006.

[20] K. Yamada et al. First demonstration of an emulsion multi-stage shifter for accelerator neutrino experiments in J-PARC T60. *PTEP*, 2017(6):063H02, 2017.

[21] Y. Suzuki, T. Fukuda, H. Kawahara, R. Komatani, M. Naiki, T. Nakano, T. Odagawa, and M. Yoshimoto. Wide angle acceptance and high-speed track recognition in nuclear emulsion. *PTEP*, 2022(6):063H01, 2022.

[22] S. Aoki et al. A Test Experiment to Develop a Neutrino Detector with Emulsions for Neutrino-Nucleus Cross Section Measurements at J-PARC. *JPS Conf. Proc.*, 8:023004, 2015.

[23] T. Odagawa, T. Fukuda, A. Hiramoto, H. Kawahara, T. Kikawa, A. Minamino, T. Nakaya, O. Sato, Y. Suzuki, and K. Yasutome. Design and performance of a scintillation tracker for track matching in nuclear-emulsion-based neutrino interaction measurement. *Nucl. Instrum. Meth. A*, 1034:166775, 2022.

[24] Y. Fukuda et al. Evidence for oscillation of atmospheric neutrinos. *Phys. Rev. Lett.*, 81:1562–1567, 1998.

[25] Q. R. Ahmad et al. Direct evidence for neutrino flavor transformation from neutral current interactions in the Sudbury Neutrino Observatory. *Phys. Rev. Lett.*, 89:011301, 2002.

[26] Claudio Giganti, Stéphane Lavignac, and Marco Zito. Neutrino oscillations: The rise of the PMNS paradigm. *Prog. Part. Nucl. Phys.*, 98:1–54, 2018.

[27] Ivan Esteban, M. C. Gonzalez-Garcia, Michele Maltoni, Thomas Schwetz, and Albert Zhou. The fate of hints: updated global analysis of three-flavor neutrino oscillations. *JHEP*, 09:178, 2020.

[28] Guido Altarelli and Ferruccio Feruglio. Discrete Flavor Symmetries and Models of Neutrino Mixing. *Rev. Mod. Phys.*, 82:2701–2729, 2010.

[29] P. H. Frampton, S. T. Petcov, and W. Rodejohann. On deviations from bimaximal neutrino mixing. *Nucl. Phys. B*, 687:31–54, 2004.

[30] M. Fukugita and T. Yanagida. Baryogenesis Without Grand Unification. *Phys. Lett. B*, 174:45–47, 1986.

[31] K. N. Abazajian et al. Light Sterile Neutrinos: A White Paper. 4 2012.

[32] Y. Farzan and M. Tortola. Neutrino oscillations and Non-Standard Interactions. *Front. in Phys.*, 6:10, 2018.

[33] K. Abe et al. The T2K Experiment. *Nucl. Instrum. Meth. A*, 659:106–135, 2011.

[34] P. I. Krastev and S. T. Petcov. Resonance Amplification and t Violation Effects in Three Neutrino Oscillations in the Earth. *Phys. Lett. B*, 205:84–92, 1988.

[35] C. Jarlskog. A Basis Independent Formulation of the Connection Between Quark Mass Matrices, CP Violation and Experiment. *Z. Phys. C*, 29:491–497, 1985.

[36] N. Abgrall et al. Measurements of $\pi^\pm$, $K^\pm$ and proton double differential yields from the surface of the T2K replica target for incoming 31 GeV/c protons with the NA61/SHINE spectrometer at the CERN SPS. *Eur. Phys. J. C*, 79(2):100, 2019.

[37] Susumu Igarashi et al. Accelerator design for 1.3-MW beam power operation of the J-PARC Main Ring. *PTEP*, 2021(3):033G01, 2021.

[38] P. A. Amaudruz et al. The T2K Fine-Grained Detectors. *Nucl. Instrum. Meth. A*, 696:1–31, 2012.
[39] K. Abe et al. T2K ND280 Upgrade - Technical Design Report. 1 2019.
[40] A. Blondel et al. A fully active fine grained detector with three readout views. *JINST*, 13(02):P02006, 2018.
[41] A. Blondel et al. The SuperFGD Prototype Charged Particle Beam Tests. *JINST*, 15(12):P12003, 2020.
[42] N. Abgrall et al. Time Projection Chambers for the T2K Near Detectors. *Nucl. Instrum. Meth. A*, 637:25–46, 2011.
[43] S. Aoki et al. The T2K Side Muon Range Detector (SMRD). *Nucl. Instrum. Meth. A*, 698:135–146, 2013.
[44] A. Blondel et al. The WAGASCI experiment at JPARC to measure neutrino cross-sections on water. *PoS*, EPS-HEP2015:292, 2015.
[45] M. Antonova et al. Baby MIND: A Magnetized Segmented Neutrino Detector for the WAGASCI Experiment. *JINST*, 12(07):C07028, 2017.
[46] Y. Fukuda et al. The Super-Kamiokande detector. *Nucl. Instrum. Meth. A*, 501:418–462, 2003.
[47] K. Abe et al. Indication of Electron Neutrino Appearance from an Accelerator-produced Off-axis Muon Neutrino Beam. *Phys. Rev. Lett.*, 107:041801, 2011.
[48] K. Abe et al. Measurements of neutrino oscillation parameters from the T2K experiment using 3.6×10^{21} protons on target. *Eur. Phys. J. C*, 83(9):782, 2023.
[49] Amanda Weltman and Anthony Walters. Viruses, microscopy and fast radio bursts: 10 remarkable discoveries from 2020. *Nature*, 588:596–598, 2020.
[50] Lars Bathe-Peters, Steven Gardiner, and Roxanne Guenette. Comparing generator predictions of transverse kinematic imbalance in neutrino-argon scattering. 1 2022.
[51] K. Abe et al. Simultaneous measurement of the muon neutrino charged-current cross section on oxygen and carbon without pions in the final state at T2K. *Phys. Rev. D*, 101(11):112004, 2020.
[52] Jaafar Chakrani. *Towards a complete understanding of neutrino-nucleus interactions with the T2K near detector upgrade*. PhD thesis, Laboratoire Leprince-Ringuet, France, Saclay, 2023.
[53] M. Martini, M. Ericson, G. Chanfray, and J. Marteau. A Unified approach for nucleon knock-out, coherent and incoherent pion production in neutrino interactions with nuclei. *Phys. Rev. C*, 80:065501, 2009.
[54] J. Nieves, I. Ruiz Simo, and M. J. Vicente Vacas. The nucleon axial mass and the MiniBooNE Quasielastic Neutrino-Nucleus Scattering problem. *Phys. Lett. B*, 707:72–75, 2012.
[55] G. D. Megias, J. E. Amaro, M. B. Barbaro, J. A. Caballero, and T. W. Donnelly. Inclusive electron scattering within the SuSAv2 meson-exchange current approach. *Phys. Rev. D*, 94:013012, 2016.
[56] I. Ruiz Simo, J. E. Amaro, M. B. Barbaro, A. De Pace, J. A. Caballero, and T. W. Donnelly. Relativistic model of 2p-2h meson exchange currents in (anti)neutrino scattering. *J. Phys. G*, 44(6):065105, 2017.
[57] J. E. Amaro, M. B. Barbaro, J. A. Caballero, T. W. Donnelly, and C. F. Williamson. Meson-exchange currents and quasielastic neutrino cross sections in the SuperScaling Approximation model. *Phys. Lett. B*, 696:151–155, 2011.
[58] J. Nieves, I. Ruiz Simo, and M. J. Vicente Vacas. Inclusive Charged–Current Neutrino–Nucleus Reactions. *Phys. Rev. C*, 83:045501, 2011.
[59] L. Alvarez-Ruso et al. NuSTEC White Paper: Status and challenges of neutrino–nucleus scattering. *Prog. Part. Nucl. Phys.*, 100:1–68, 2018.
[60] J. E. Sobczyk, J. Nieves, and F. Sánchez. Exclusive-final-state hadron observables from neutrino-nucleus multinucleon knockout. *Phys. Rev. C*, 102(2):024601, 2020.
[61] J. E. Sobczyk and J. Nieves. Neutrino and antineutrino charged-current multi-nucleon cross sections revisited. 7 2024.
[62] Hemant Prasad, Jan T. Sobczyk, Artur M. Ankowski, J. Luis Bonilla, Rwik Dharmapal Banerjee, Krzysztof M. Graczyk, and Beata E. Kowal. New multinucleon knockout model in NuWro Monte Carlo generator. 11 2024.
[63] Lukas Berns. First results from the joint oscillation analysis between SK atmospheric neutrinos and T2K accelerator neutrinos. J-PARC / KEK Seminar, 12 2023.
[64] N. Latham. First measurement of the charged current electron neutrino pion production cross section on a carbon target at t2k. 2024.
[65] Wissal Filali, Laura Munteanu, and Stephen Dolan. Benchmarking neutrino interaction models via a comparative analysis of kinematic imbalance measurements from the T2K, MicroBooNE and MINERvA experiments. 7 2024.
[66] K. Abe et al. First T2K measurement of transverse kinematic imbalance in the muon-neutrino charged-current single-π^+ production channel containing at least one proton. *Phys. Rev. D*, 103(11):112009, 2021.
[67] Alain Boudard, Joseph Cugnon, Jean-Christophe David, Sylvie Leray, and Davide Mancusi. New potentialities of the Liège intranuclear cascade model for reactions induced by nucleons and light charged particles. *Phys. Rev. C*, 87(1):014606, 2013.
[68] J. L. Rodríguez-Sánchez, J. Cugnon, J. C. David, J. Hirtz, A. Kelić-Heil, and S. Leray. Hypernuclei formation in spallation reactions by coupling the Liège intranuclear cascade model to the deexcitation code ABLA. *Phys. Rev. C*, 105(1):014623, 2022.
[69] Nuwro official repository. `https://github.com/NuWro/nuwro`.
[70] A. Ershova et al. Role of deexcitation in the final-state interactions of protons in neutrino-nucleus interactions. *Phys. Rev. D*, 108(11):112008, 2023.
[71] K. Abe et al. First combined measurement of the muon neutrino and antineutrino charged-current cross section without pions in the final state at T2K. *Phys. Rev. D*, 101(11):112001, 2020.
[72] D. Ruterbories et al. Measurement of Quasielastic-Like Neutrino Scattering at $\langle E_\nu \rangle \sim 3.5$ GeV on a Hydrocarbon Target. *Phys. Rev. D*, 99(1):012004, 2019.
[73] P. A. Rodrigues et al. Identification of nuclear effects in neutrino-carbon interactions at low three-momentum transfer. *Phys. Rev. Lett.*, 116:071802, 2016. [Addendum: Phys.Rev.Lett. 121, 209902 (2018)].
[74] O. Benhar, A. Fabrocini, S. Fantoni, and I. Sick. Spectral function of finite nuclei and scattering of GeV electrons. *Nucl. Phys. A*, 579:493–517, 1994.
[75] Teppei Katori and Marco Martini. Neutrino–nucleus cross sections for oscillation experiments. *J. Phys. G*, 45(1):013001, 2018.
[76] A. Hiramoto. *Ph. D. thesis, Kyoto University*, 2021.
[77] A. Alekou et al. The European Spallation Source neutrino super-beam conceptual design report. *Eur. Phys. J. ST*, 231(21):3779–3955, 2022. [Erratum: Eur.Phys.J.ST 232, 15–16 (2023)].

[78] A. Alekou et al. The ESSnuSB Design Study: Overview and Future Prospects. *Universe*, 9(8):347, 2023.
[79] Babak Abi et al. Deep Underground Neutrino Experiment (DUNE), Far Detector Technical Design Report, Volume II: DUNE Physics. 2 2020.
[80] S. Navas et al. Review of particle physics. *Phys. Rev. D*, 110(3):030001, 2024.
[81] C. Andreopoulos et al. The GENIE Neutrino Monte Carlo Generator. *Nucl. Instrum. Meth. A*, 614:87–104, 2010.
[82] Costas Andreopoulos, Christopher Barry, Steve Dytman, Hugh Gallagher, Tomasz Golan, Robert Hatcher, Gabriel Perdue, and Julia Yarba. The GENIE Neutrino Monte Carlo Generator: Physics and User Manual. 10 2015.
[83] Júlia Tena-Vidal et al. Neutrino-Nucleon Cross-Section Model Tuning in GENIE v3. 4 2021.
[84] Luis Alvarez-Ruso, Joshua L Barrow, Leo Bellantoni, Minerba Betancourt, Alan Bross, Linda Cremonesi, Kirsty Duffy, Steven Dytman, Laura Fields, Tsutomu Fukuda, et al. Neutrino scattering measurements on hydrogen and deuterium: A snowmass white paper. *arXiv preprint arXiv:2203.11298*, 2022.
[85] T. Neff H. Feldmeier, W. Horiuchi and Y. Suzuki. Universality of short-range nucleon-nucleon correlations. *Phys. Rev. C*, 84:054003, 2011.
[86] R.J. Furnsthl M.A. Hisham A. Lovato R.B. Wiringa A. J. Tropiano, S. K. Bogner. High-resolution momentum distributions from low-resolution wave functions. *Physical Letters B*, 852:138591, 2024.
[87] G. Shen, L. E. Marcucci, J. Carlson, S. Gandolfi, and R. Schiavilla. Inclusive neutrino scattering off deuteron from threshold to GeV energies. *Phys. Rev. C*, 86:035503, 2012.
[88] S. Nakamura, T. Sato, Vladimir P. Gudkov, and K. Kubodera. Neutrino reactions on deuteron. *Phys. Rev. C*, 63:034617, 2001. [Erratum: Phys.Rev.C 73, 049904 (2006)].
[89] S. X. Nakamura, H. Kamano, and T. Sato. Impact of final state interactions on neutrino-nucleon pion production cross sections extracted from neutrino-deuteron reaction data. *Phys. Rev. D*, 99(3):031301, 2019.
[90] K. Abe et al. *Nucl. Instrum. Meth. Phys. Res. A*, 694:211–223, 2012.
[91] M. Otani. *Ph. D. thesis, Kyoto University*, 2012.
[92] R. Acciarri, C. Adams, J. Asaadi, B. Baller, T. Bolton, C. Bromberg, F. Cavanna, E. Church, D. Edmunds, A. Ereditato, S. Farooq, B. Fleming, H. Greenlee, G. Horton-Smith, C. James, E. Klein, K. Lang, P. Laurens, R. Mehdiyev, B. Page, O. Palamara, K. Partyka, G. Rameika, B. Rebel, M. Soderberg, J. Spitz, A. M. Szelc, M. Weber, T. Yang, and G. P. Zeller. Detection of back-to-back proton pairs in charged-current neutrino interactions with the argoneut detector in the numi low energy beam line. *Phys. Rev. D*, 90:012008, Jul 2014.
[93] M. A. Acero et al. White Paper on Light Sterile Neutrino Searches and Related Phenomenology. 3 2022.
[94] A. Aguilar et al. Evidence for neutrino oscillations from the observation of $\bar{\nu}_e$ appearance in a $\bar{\nu}_\mu$ beam. *Phys. Rev. D*, 64:112007, 2001.
[95] A. A. Aguilar-Arevalo et al. Updated MiniBooNE neutrino oscillation results with increased data and new background studies. *Phys. Rev. D*, 103(5):052002, 2021.
[96] C. Giunti, Y. F. Li, C. A. Ternes, and Z. Xin. Reactor antineutrino anomaly in light of recent flux model refinements. *Phys. Lett. B*, 829:137054, 2022.
[97] Mario A. Acero, Carlo Giunti, and Marco Laveder. Limits on nu(e) and anti-nu(e) disappearance from Gallium and reactor experiments. *Phys. Rev. D*, 78:073009, 2008.
[98] P. Abratenko et al. Search for an Excess of Electron Neutrino Interactions in MicroBooNE Using Multiple Final-State Topologies. *Phys. Rev. Lett.*, 128(24):241801, 2022.
[99] A. A. Aguilar-Arevalo et al. MiniBooNE and MicroBooNE Combined Fit to a 3+1 Sterile Neutrino Scenario. *Phys. Rev. Lett.*, 129(20):201801, 2022.
[100] V. V. Barinov et al. Results from the Baksan Experiment on Sterile Transitions (BEST). *Phys. Rev. Lett.*, 128(23):232501, 2022.
[101] A. P. Serebrov et al. Search for sterile neutrinos with the Neutrino-4 experiment and measurement results. *Phys. Rev. D*, 104(3):032003, 2021.
[102] R. Abbasi et al. Exploration of mass splitting and muon/tau mixing parameters for an eV-scale sterile neutrino with IceCube. 6 2024.
[103] P. Adamson et al. Improved Constraints on Sterile Neutrino Mixing from Disappearance Searches in the MINOS, MINOS+, Daya Bay, and Bugey-3 Experiments. *Phys. Rev. Lett.*, 125(7):071801, 2020.
[104] K. Abe et al. Search for light sterile neutrinos with the T2K far detector Super-Kamiokande at a baseline of 295 km. *Phys. Rev. D*, 99(7):071103, 2019.
[105] M. A. Acero et al. Dual-Baseline Search for Active-to-Sterile Neutrino Oscillations in NOvA. 9 2024.
[106] H. Almazán et al. Joint Measurement of the ^{235}U Antineutrino Spectrum by Prospect and Stereo. *Phys. Rev. Lett.*, 128(8):081802, 2022.
[107] Y. J. Ko et al. Sterile Neutrino Search at the NEOS Experiment. *Phys. Rev. Lett.*, 118(12):121802, 2017.
[108] R. Abbasi et al. Search for a light sterile neutrino with 7.5 years of IceCube DeepCore data. 7 2024.
[109] Supraja Balasubramanian. Beyond the Standard Model New Physics Searches with SBND †. *Phys. Sci. Forum*, 8(1):68, 2023.
[110] P. Abratenko et al. ICARUS at the Fermilab Short-Baseline Neutrino program: initial operation. *Eur. Phys. J. C*, 83(6):467, 2023.
[111] Monojit Ghosh, Tommy Ohlsson, and Salvador Rosauro-Alcaraz. Sensitivity to light sterile neutrinos at ESSnuSB. *JHEP*, 03:026, 2020.
[112] P. Abratenko et al. First Constraints on Light Sterile Neutrino Oscillations from Combined Appearance and Disappearance Searches with the MicroBooNE Detector. *Phys. Rev. Lett.*, 130(1):011801, 2023.